AI-assisted decoding of molecular signatures essential for condensation and function of NON-PHOTOTROPIC HYPOCOTYL3

Prabha Manishankar, Lea Reuter, Atiara Fernandez, Yeliz Idil Yigit, Jutta Keicher, Andrea Bock, Claudia Oecking*

Center for Plant Molecular Biology (ZMBP), Plant Physiology, University of Tübingen, Tübingen, Germany.

* Contact. Email: claudia.oecking@zmbp.uni-tuebingen.de

ABSTRACT

The plasma membrane associated protein NON-PHOTOTROPIC HYPOCOTYL 3 (NPH3) is a key component of the auxin-dependent phototropic growth response in plants. Blue light induces the detachment of NPH3 from the plasma membrane into the cytosol, where it dynamically transitions into membrane-less biomolecular condensates. Despite the importance of NPH3/RPT2-Like (NRL) proteins for developmental plasticity of plants, little is known about their structure-function relationship. Here, we combine experimental data with the power of AI-based protein structure prediction to uncover molecular signatures of NPH3. Our approach unveils a bipartite C-terminal motif that enables self-interaction of NPH3 with different strengths. We further demonstrate that the C-terminal homo-oligomerization is required for both association with the plasma membrane and condensate assembly, with a different part of the bipartite motif playing the key role in each case. However, multivalency-driven transition of NPH3 to the condensed state depends on the co-operative action of an N-terminal NPH3 signature. We propose that NPH3 is a single hub that can form a polymerized network based on two distinct structural domains that self-associate. NPH3 variants that are incapable of condensation are non-functional, suggesting a fundamental role of phase separation of NPH3 for auxin-dependent phototropism. This structural snapshot may have direct implications on future analyzes of NRL family members.

Introduction

The phototropic response describes the capability of plants to re-orient shoot growth towards a directional blue light (BL) source which ultimately enhances photosynthetic competence. The BL-activated and plasma membrane (PM)-associated AGCVIII kinases, phototropin1 (phot1) and phot2, function as primary photoreceptors and the asymmetric growth of the hypocotyl is based on the establishment of a lateral auxin gradient with a higher hormone concentration on the shaded side[1-5]. In this context, it is not surprising that certain members of the PIN-FORMED (PIN) family of auxin efflux carriers are required for phototropic hypocotyl bending[6]. In addition to the regulation of PIN activity by a family of AGCVIII protein kinases (D6 PROTEIN KINASES)[6,7], alterations in the subcellular polarity of PIN proteins, particularly PIN3[8,9], are known to mediate the effect of BL on auxin distribution[2,3,10]. Although the mechanism linking photoreceptor activation to PIN protein modulation is still unknown, recent data have revealed that dynamic changes in the subcellular localization of the early phototropic signaling component NON-PHOTOTROPIC HYPOCOTYL 3 (NPH3) are crucial for phot1 signaling[11,12] and thus for auxin redistribution[2,3,10-12]. In darkness, NPH3 associates to the PM[13,14] in a phospholipid-dependent manner[11] and physically interacts with the photoreceptor phot1[13,15]. Following BL perception, phot1 directly phosphorylates[12] the third last residue (S744) of NPH3, which represents a C-terminal 14-3-3 binding motif[11,12].

Subsequent association of 14-3-3 proteins is causal for the light-induced release of NPH3 from the PM into the cytosol[11,12], where it dynamically transitions into membrane-less condensate-like particles[11]. Intriguingly, the light-induced processes are reversible, eventually resulting in PM reassociation of NPH3[11,16]. Moreover, NPH3 mutants constitutively localizing to either the PM or condensates show compromised functionality, consistent with a model where phototropic curvature critically depends on the 14-3-3 mediated dynamic change in NPH3 localization, ultimately leading to a gradient of NPH3 subcellular localization across the hypocotyl[11,12].

Together with ROOT PHOTOTROPISM 2 (RPT2), NPH3 is the founding member of the plant-specific NPH3/RPT2-Like (NRL) protein family consisting of 33 members in Arabidopsis[17,18]. Several of them act – comparable to NPH3 - as signal transducers in processes involving auxin (re)distribution in response to developmental or environmental cues, most likely via regulation of PIN auxin carriers[19-22]. Indeed, MAB4/ ENP-like (MEL) polypeptides were recently shown to maintain PIN polarity by limiting lateral diffusion[23]. Considering that several NRL proteins are potential direct substrate targets of the phot AGCVIII kinases[12,24] and furthermore are able to interact with 14-3-3 via the corresponding phosphorylated motif[11], phosphorylation-dependent 14-3-3 association may represent a more general regulatory mechanism. Noteworthy, in addition to localization at the PM, MEL proteins also form particle-like structures in the cytosol[21,23,25] that are reminiscent of resemble NPH3 condensates.

Membrane-less biomolecular condensates are emerging as a fundamental mechanism to compartmentalize cellular functions. In plants, condensate assembly appears to integrate environmental cues with development[26,27] and their formation is driven by multivalent macromolecular interactions[28-30]. NRL family members are mostly characterized by a central NPH3 domain and two putative protein interaction domains, namely an N-terminal bric-a-brac, tramtrack and broad complex (BTB) domain and a C-terminal coiled-coil (CC) domain[18]. As yet, our understanding of the structure-function relationship is very limited, making it impossible to address the important question of whether condensate formation of PM-detached NPH3 is essential for its action. Accurately modeling the structures of proteins and their complexes using artificial intelligence (AI) is revolutionizing molecular biology[31,32]. Here, we closely link experimental data and AI-assisted protein structure predictions to decipher the molecular functions of the structured NPH3 domains. We report the identification of a bipartite C-terminal self-association motif required for both PM association of NPH3 in darkness and BL-triggered condensate assembly in the cytosol. The bipartite motif consists of the CC domain and an as yet undescribed Linear Interacting Peptide (LIP) localized at the C-terminal end of the NPH3 domain. Remarkably, only the LIP-mediated self-association of NPH3 with low affinity is essential for the transition to the

condensed state. In addition, the BTB domain contributes directly to the oligomeric states of NPH3 in cytoplasmic assemblies. Overall, we propose the conversion of a strict C-terminal self-association of NPH3 at the PM into a cooperative LIP/BTB mediated polymerization in the cytosol. Intriguingly, several NPH3 variants incapable of condensate formation are non-functional, suggesting that the temporal regulation of the BL-induced NPH3 cycling between the PM and the cytosol is critical for its function in auxin-dependent phototropism.

Results

NPH3 self-associates independently of its subcellular localization and its BTB domain

According to protein signature models NPH3 possesses an N-terminal BTB, a central NPH3 and a C-terminal CC domain[18]. Structure prediction by AlphaFold2 (AF2)[31] or AF3[33], AI-based tools, confirmed the above domains, each characterized by defined secondary structures and high confidence scores (per residue predicted Local Distance Difference Test, pLDDT) (Fig. 1a and Supplementary Fig. 1a). Additionally, six intrinsically disordered regions (IDR), showing low pLDDT values and covering about 40% of the protein, are distributed along the entire length of NPH3 (Fig. 1a and Supplementary Fig. 1a). Despite this, the positions (Predicted Aligned Error, PAE) of the structured domains relative to each other are well-defined – except for the CC domain (Supplementary Fig. 1b).

Protein condensate formation relies on multivalent interactions. Since NPH3 mutants that constitutively form cytosolic condensates (NPH3ΔC51, NPH3_4K/A) strictly co-localize when transiently co-expressed in *N. benthamiana* leaves[11] (Fig. 1b), we wondered whether NPH3 associates with itself in cytoplasmic assemblies. Stringent CoIP of fluorophore-tagged proteins confirmed their physical association (Fig. 1c). However, NPH3 self-association is not restricted to cytosolic assemblies but also occurs at the PM (NPH3/NPH3 darkness, Fig. 1b, c). Remarkably, the condensate-localizing RFP:NPH3ΔC51 uniformly associates with the PM in the dark when co-expressed with GFP:NPH3 (Fig. 1b), implying that self-association of NPH3 enables the relocation of cytosolic variants to the PM. This phenomenon is hereafter referred to as self-association linked to relocation. Subsequent BL irradiation triggered co-localization of RFP:NPH3ΔC51 and GFP:NPH3 in cytosolic assemblies (Fig. 1b). Conversely, PM retention in BL was observed when RFP:NPH3ΔC51 or RFP:NPH3 were co-expressed with the constitutively PM-localized GFP:NPH3-S744A mutant[11,12] (Supplementary Fig. 1c). In each case, interaction of NPH3 mutant variants was validated by Co-IP (Fig. 1c and Supplementary Fig. 1d). The BTB domain has often been associated with homo- or hetero-multimerization of NRL family members[1,17,34,35]. However, deletion of the BTB domain (NPH3ΔN197) had no effect on homo-oligomerization at the PM or the ability to translocate RFP:NPH3ΔC51 to the PM in darkness (Fig. 1b, c and Supplementary Fig. 1c). Consequently, BTB-independent self-association of NPH3 at the PM (dark) might be coupled

to the dynamic formation of higher-order homo-or hetero-oligomers in the cytosol (BL), eventually leading to phase separation.

AlphaFold2-multimer assisted identification of a bipartite C-terminal self-association motif

We next examined whether the CC domain of NPH3 contributes directly to self-association linked to relocation. When NPH3 truncated by the CC domain (NPH3ΔC104) was co-expressed with NPH3 in darkness, it formed condensate-like particles near the PM (Fig. 2a) – an obvious difference to the uniform PM localization of NPH3ΔC51 (Fig. 1b). In BL, however, NPH3ΔC104 mirrors NPH3ΔC51, as it co-localizes with NPH3 or NPH3ΔC51 in cytosolic condensates (Fig. 2a and Supplementary Fig 2a). Stringent CoIP revealed that NPH3ΔC104 – as compared to NPH3ΔC51 - interacted significantly weaker with NPH3 or NPH3ΔC51, albeit complex formation was still detectable (Fig. 2b and Supplementary Fig. 2b). We thus hypothesized that the CC domain promotes a high-affinity interaction essential for self-association linked to relocation. By contrast, the remaining weak interaction capability of NPH3ΔC104 might be sufficient to contribute to multivalency-driven condensate assembly. To unveil potential homomeric NPH3 interfaces, AF2-Multimer (AF2M), a protein complex structure prediction tool[32], or alternatively AF3[33] was used. However, confidence scores (pLDDT) of the AF3 prediction were lower than those of AF2M – most likely due to the high number of disordered regions in NPH3 (see AlphaFold server, limitations of the AF3 model). As the models did not differ in principle, the AF2M predictions are shown. NPH3 is predicted to form a trimer stabilized by the CC super helices (Fig. 2c, Supplementary Fig. 2c). Since the amphipathic helix required for PM association (arrowhead Fig. 2c center) is found in the adjacent downstream region[11], the CC trimer is most likely located near the PM. Excitingly, upstream of the CC trimer, AF2M predicts another three-helical bundle. Here, a Linear Interacting Peptide (LIP) (MobiDB: $_{592}$LRV**VVQVLF**, highlighted in yellow in all ribbon plots and schemes of NPH3) might establish hydrophobic helix-helix interfaces. The so far unrecognized LIP represents the (almost) C-terminal end of the central NPH3 domain, exhibiting high sequence identity within the NRL protein family[15] (Supplementary Fig. 2d). In each trimeric NPH3 subunit, the entire region encompassing the BTB and NPH3 domains, including LIP, adopts a conformation close to that of the NPH3 monomer, while the position of the CC appears to be flexible in relation to the rest of the protein (PAE plot, Supplementary Fig. 2c). As a consequence of the putative LIP interactions, the NPH3 trimer exhibits a nearly perfect rectangular arrangement of its monomeric subunits. A view from below shows a symmetrically arranged 3-bladed propeller with the LIP-trimer in its center (Fig. 2c bottom).

We first validated our hypothesis of CC-mediated high-affinity self-association of NPH3 linked to relocation by replacing three hydrophobic residues (Fig. 2d: W650, L664, M681) with glutamic acid (NPH3_WLM/E) to destabilize the CC superstructure. Indeed, GFP:NPH3_WLM/E failed to uniformly relocate RFP:NPH3ΔC51 to the PM in darkness (Fig. 2d) and its ability to bind NPH3ΔC51 was significantly impaired compared to GFP:NPH3 (Fig. 2b). However, both proteins colocalized in cytoplasmic assemblies upon BL treatment (Fig. 2d), reflecting the joint expression of PM-associated NPH3 and cytosolic NPH3ΔC104 lacking the CC domain (Fig. 2a). Overall, the CC domain is essential for the high-affinity self-association of NPH3 linked to relocation.

Based on the structural prediction, the LIP motif may represent the molecular signature allowing for weak interaction and potentially condensate formation of NPH3 variants impaired in CC-mediated high-affinity interaction (NPH3ΔC104, NPH3_WLM/E). Notably, AF2M still predicts the formation of a trimer for NPH3ΔC104, with high confidence scores for LIP residues at the trimer interface (Supplementary Fig. 2e). By contrast, trimer formation is not supported by AF2M if the LIP motif is additionally truncated (NPH3ΔC164). Co-expression analyzes demonstrated a mainly cytosolic localization of NPH3ΔC164 and a clear separation from the strictly condensate-forming NPH3ΔC51 as well as from NPH3 both in darkness and upon BL irradiation (Fig. 2a and Supplementary Fig. 2a). Moreover, comparative CoIP analyzes revealed a clear stepwise decrease in affinity: compared to NPH3ΔC51, deletion of the CC (NPH3ΔC104) leads to a significant decrease in interaction, while additional truncation of the LIP motif (NPH3ΔC164) almost abolished complex formation with both NPH3 and NPH3ΔC51 (Fig. 2b and Supplementary Fig. 2b). We therefore propose a bipartite C-terminal self-association motif in NPH3 consisting of the CC domain which mediates high-affinity homo-oligomerization required for relocation, and the LIP motif, which allows a low-affinity interaction apparently sufficient to contribute to the transition of NPH3 to the condensed state in the cytosol.

The bipartite C-terminal self-association motif is required for plasma membrane recruitment of NPH3 in darkness

To validate the trimerization of the CC domain predicted by AF2M, size exclusion chromatography of recombinant C-terminal NPH3 fragments tagged with $(His)_6$-maltose-binding protein (MBP) was performed. While the MBP:NPH3-C51 (C-terminal 51 residues) fusion protein (calculated MW: 48.2 kDa) eluted at a volume indicative of a monomer (15 ml, approx. 47 kDa), the presence of the CC domain (MBP:NPH3-C104, C-terminal 104 residues, calculated MW: 54.4 kDa) shifted the elution peak significantly, corresponding to a native molecular weight of a trimer (12 ml, approx. 166 kDa) (Fig. 3a, Supplementary Fig. 3). Worth mentioning, destabilization of the CC superstructure (MBP:NPH3-C104_WLM/E)

clearly interferes with trimer formation and likely leads to a monomeric state (14 ml, approx. 74 kDa) (Fig. 3a). In summary, the CC domain of NPH3 assembles into a stable trimer *in vitro,* supporting the AF2M prediction.

What's the molecular role of NPH3 trimer formation? The region downstream of the CC, NPH3-C51, contains the amphipathic helix crucial for phospholipid-dependent PM association. Despite its direct binding to phospholipids *in vitro*[11], GFP:NPH3-C51 surprisingly failed to associate with the PM *in vivo* (Fig. 3b). However, extension by the trimeric CC domain (GFP:NPH3-C104) enabled PM association in darkness (Fig. 3b), as confirmed by subcellular fractionation (Fig. 3c). Membrane targeting of GFP:NPH3-C104 is in turn impaired when formation of CC trimers (GFP:NPH3-C104_WLM/E) or alternatively phospholipid binding of NPH3 (GFP:NPH3-C104_4K/A, see[11]) is reduced (Fig. 3b, c). Thus, PM recruitment of NPH3 in darkness requires both homo-oligomerization and phospholipid interaction.

Analysis of full-length NPH3 variants aimed to understand the role of the LIP motif in PM attachment. Deletion of the 9 aa comprising LIP motif ($_{592}$LRV**VVQVLF**) served as a means to prevent the LIP-mediated low-affinity homo-oligomerization (GFP:NPH3ΔLIP) and had no apparent effect on PM association (Fig. 3b, c). Disruption of CC trimer assembly shifted a significant proportion of GFP:NPH3_WLM/E to the soluble fraction following subcellular fractionation but the shift was substantially smaller compared to NPH3-C104_WLM/E lacking the LIP motif (Fig. 3c). Remarkably, the full-length GFP:NPH3_WLM/E clearly localizes to the cell periphery, suggesting weak PM attachment *in vivo,* likely due to LIP-mediated low-affinity self-association. Indeed, loss of PM recruitment could only be observed when the self-association of both parts of the bipartite structured motif was impaired (GFP:NPH3ΔLIP_WLM/E, Fig. 3b, c).

Overall, we concluded that the bipartite C-terminal self-association motif acts unequally redundant in terms of membrane recruitment of NPH3 with the CC domain fully compensating for loss of the LIP motif. However, when CC trimerization is impaired, the LIP motif partially compensates, facilitating weak PM association of NPH3, probably due to low-affinity self-association.

Deciphering molecular signatures of NPH3 essential for condensate formation of NPH3

Biomolecular condensates typically form via liquid-liquid phase separation, and their formation relies on multivalent molecules. Multivalency in proteins can be achieved by structured interaction domains, IDRs or a combination of both[29].

We have recently reported that BL irradiation initially triggers re-localization of NPH3 from the PM to the cytosol, where it dynamically transitions to a condensed state. While 14-3-3

association is critical for initial PM detachment of NPH3, it is dispensable for condensate assembly. Phase separation could therefore be an autonomous process as soon as a critical cytosolic NPH3 concentration is reached[11].

Our co-expression data suggested that deletion of the C-terminal bipartite motif prevents condensate formation (NPH3ΔC164, Fig. 2a). Single expression of NPH3ΔC164 confirmed the direct contribution of the bipartite motif to the oligomeric states of NPH3 in cytoplasmic assemblies (Fig. 4a, Supplementary Fig. 4a). However, exclusive interference with CC formation (NPH3ΔC104, NPH3_WLM/E) only marginally affected condensate assembly of NPH3. Unexpectedly, deletion of the LIP motif alone (NPH3ΔLIP) abolished transition of cytosolic NPH3 to the condensed state (Fig. 4a). Replacement of four hydrophobic/uncharged residues potentially involved in hydrophobic LIP-LIP interfaces with alanine or glutamic acid ($_{592}$LRV**VVQVLF**SEQ ⇒ $_{592}$ERV**VAQVEF**SEA) (NPH3_4LVQ/EA, Supplementary Fig. 4b) revealed that lack of homotypic LIP interactions is causal for the loss of phase separation ability of NPH3ΔLIP (Fig. 4a). Taken together, the CC domain and the LIP motif act non-redundantly in condensate formation of NPH3: here, the LIP motif is instrumental, while the CC is dispensable.

Multivalency describes the ability to participate in multivalent interactions. Deletion of the BTB domain (GFP:NPH3ΔN197) had no effect on high-affinity self-association of NPH3 at the PM (Fig. 1b, c) but proved incapable of BL-triggered phase separation in the cytosol (Fig. 4a, Supplementary Fig 4a), indicating that it represents another essential NPH3 interaction valence. Collectively, BTB-independent self-association of NPH3 at the PM (dark) seems be coupled to the dynamic formation of BTB-dependent higher-order homo- or hetero-oligomers in the cytosol (BL).

The BTB domain of NRL protein family members is characterized by a conserved alpha-helical extension at the C-terminus (α6 - α8, highlighted in light blue in all ribbon plots and schemes of NPH3) of the core BTB fold (β-sheets B1-B3, α-helices A1-A5)[36]. BTB domains enable protein-protein interactions, including multimerization and interactions with non-BTB proteins[37]. However, interaction partners of NPH3 that are enriched in cytosolic condensates have not yet been identified, with the exception of 14-3-3 proteins[12] (own unpublished results), but these are not relevant for phase separation[11]. We therefore suspected that NPH3 forms a single-component condensate that may include associated proteins such as 14-3-3. This in turn implies that the BTB domain can also establish homotypic interactions. AF2M provides evidence that NPH3ΔC164 could form dimers via its BTB domain (Fig. 4b, Supplementary Fig. 4c). Given the reversibility of condensate formation[11,13], the putative BTB-BTB interaction is most likely weak and occurs spontaneously. NPH3 could therefore be a single hub that can homopolymerize via two distinct structural domains in its N- and C-terminus, respectively. In this context, it is of particular importance that the BTB domains

appear to dimerize in an antiparallel manner (Fig. 4b). Consequently, cross-linking of individual NPH3 trimers via BTB-mediated antiparallel interactions could enable the formation of higher-order network-like assemblies (Supplementary Fig. 4d, e).
The hypothetical antiparallel BTB-BTB interaction relies on hydrophobic interactions between helices A5 of the core BTB and α8 of the C-terminal extension. Deletion of the C-terminal extension (NPH3ΔBTBα6-8) or helix α8 alone (NPH3ΔBTBα8) prevented NPH3 condensation (Fig. 4c). The C-terminal extension of the plant-specific BTB domain is thus crucial for polymerization of NPH3 in the cytosol. However, we cannot exclude that non-BTB proteins or BTB proteins different from NPH3 are involved in and required for the formation of cytoplasmic NPH3 assemblies.
Finally, why does disruption of the hydrophobic LIP-LIP interfaces (NPH3ΔLIP/NPH3_4LVQ/EA) abolish phase transition of NPH3, despite the presence of the trimeric CC domain and the BTB domain? According to the AF2M prediction, deletion of the LIP motif causes a breakdown of the symmetric right-angle conformation of the individual NPH3 monomers within the trimer. As a result, the three BTB domains are in close contact to each other, with helices A5 and α8 of the individual monomers facing each other (Supplementary Fig. 4f). We therefore assume that the formation of antiparallel BTB-BTB interactions is almost impossible.

Phot1-dependent dephosphorylation of NPH3 does neither require condensate formation nor PM dissociation

Based on our novel data, we addressed open questions regarding the complex phosphorylation changes of NPH3. In dark-grown seedlings, multiple residues in the N-terminal IDRs of the PM-associated NPH3 are phosphorylated independently of the photoreceptor phot1[38-40]. BL induces an immediate phosphorylation of the third-last residue of NPH3 (S744), triggering association with 14-3-3, followed by PM release of NPH3 and dephosphorylation of the N-terminal residues[11,12]. This light-induced and phot1-dependent dephosphorylation of NPH3 is visualized by a slight shift in electrophoretic mobility of NPH3[13,38-40].
As yet it is still unknown whether phot1-dependent dephosphorylation requires PM dissociation and/or phase transition of NPH3 in the cytosol. Despite the inability of NPH3ΔN197, GFP:NPH3ΔBTBα8 and NPH3ΔLIP to form condensates, BL irradiation induces (i) phosphorylation of their third last residue (Fig. 5a) and (ii) PM-detachment (Supplementary Fig. 5). In addition, a shift in electrophoretic mobility is evident, demonstrating their phot1-dependent dephosphorylation. Furthermore, all light-induced processes are reverted upon re-transfer to darkness (Fig. 5a), eventually leading to PM re-association of the condensate-incompetent variants (Supplementary Fig. 5). Overall, we

concluded (i) that condensation is not required for the dephosphorylation of NPH3 observed upon phot1 activation and (ii) that all analyzed NPH3 variants exhibit the properties typical for NPH3, with the exception of phase separation in the cytosol.
However, the condensate-localizing NPH3-4K/A mutant is constitutively dephosphorylated in transgenic Arabidopsis seedlings[11] as well as in transiently expressing *N. benthamiana* leaves (Fig. 5b). Thus, either phot1-dependent dephosphorylation is linked to cytosolic localization of NPH3 or phot1-independent phosphorylation of NPH3-IDRs requires PM localization. We therefore relocated NPH3-4K/A to the PM in the dark by simultaneous expression with NPH3 (Fig. 5c). PM association resulted in a substantial portion of NPH3-4K/A exhibiting reduced electrophoretic mobility indicative of phosphorylation (Fig. 5b). It is worth mentioning that BL irradiation triggers dephosphorylation of NPH3-4K/A, not only when co-expressed with NPH3, but also with NPH3-S744A which keeps NPH3-4K/A attached to the PM (Fig. 5b, c). In summary, phot1-independent phosphorylation in the dark requires PM association of NPH3, whereas PM dissociation is dispensable for phot1-dependent dephosphorylation.

Condensate formation of NPH3 might be key to function

Recent studies have emphasized the critical role of light-triggered NPH3 cycling between the PM and the cytosol in phototropism[11,12]. However, the functional relevance of NPH3 phase separation in the cytosol remains unclear. As previously described, GFP:NPH3 was fully functional in restoring the severe impairment of hypocotyl phototropism in *nph3-7*, regardless of whether expression was driven by the endogenous or the 35S promoter[11-14]. By contrast, ectopic expression of condensation-incapable NPH3 variants (GFP:NPH3ΔN197, GFP:NPH3ΔBTBα8, GFP:NPH3ΔLIP) failed to complement the phenotype (Fig. 6a), suggesting that NPH3 phase separation is of importance for NPH3 function. However, NPH3ΔN197 completely lacks the BTB domain, and deletion of the LIP motif (NPH3ΔLIP) could indirectly affect BTB-dependent interactions through conformational rearrangement (Supplementary Fig. 4f). The limited function of these variants might thus alternatively be caused by loss of an essential BTB-dependent NPH3 interaction partner. A prime candidate in this regard is RPT2, which is required for hypocotyl phototropism[13] and has been reported to interact with NPH3 via the BTB domain. In this context, the isolated N-terminal domains of the respective proteins were used in a yeast two hybrid assay[35]. By contrast, stringent CoIP of fluorophore-tagged proteins demonstrated that the physical association of the two NRL family members is not affected by deletion of the BTB domain of NPH3 (Fig. 6b). We therefore concluded that RPT2 associates with NPH3 *in planta* independent of its BTB domain. Considering that the typical features of NPH3 in terms of phosphorylation status and changes in subcellular localization are conserved in all phase transition-incapable NPH3

variants (Fig. 5a, Supplementary Fig. 5, Fig. 6c), the most likely cause of their impaired function is the inability to form condensates. In this context we assume that condensation serves to sequester NPH3 in the cytosol and thus keep it away from the PM. Considering the reversibility of this process, the balanced temporal regulation of NPH3 cycling between the PM and the cytosol seems to be central to phototropic hypocotyl bending.

Discussion

Our data provide novel insights into molecular signatures of NPH3 defining its characteristics and function in BL-induced phototropic hypocotyl bending. We applied a combination of live-cell imaging, deep learning-based structure prediction, biochemical, genetic and physiological approaches to uncover unique, overlapping and cooperative roles of NPH3 motifs essential for self-association at the PM and/or the formation of multivalency-driven condensates in the cytosol. Members of the NRL protein family are mostly characterized by three domains, the N-terminal BTB-, the central NPH3 domain and the C-terminal CC domain, all of which are known since decades[15]. However, our understanding of structure-function relationship of NRL's is quite limited.

In vivo protein-protein interaction assays, combined with confocal imaging of *N. benthamiana* leaf epidermis cells expressing NPH3 variants revealed the crucial role of the CC domain in mediating high-affinity self-association of NPH3 at the PM (Fig. 2a, b). Though deletion/destabilization of the CC (NPH3ΔC104/NPH3-WLM/E) substantially impaired the interaction strength, weak homo-oligomerization and, above all, condensate formation could still be observed (Fig. 2a, b, Fig. 4a). AF2M predicted the formation of NPH3 trimers and provided previously unexpected molecular insights that eventually led to the discovery of a bipartite C-terminal self-association motif. In fact, the trimeric NPH3 complex appears to be stabilized by (i) the CC superhelices and additionally by (ii) a helical bundle formed by an as yet unrecognized upstream feature, the LIP motif (Fig. 2c). Experimental validation confirmed the formation of trimers by the CC domain (Fig. 3a) and emphasized the role of the LIP motif in establishing low-affinity homomeric contacts (NPH3ΔC104 vs. NPH3ΔC164, Fig. 2b, Supplementary Fig. 2b). The LIP motif localizes to the C-terminal end of the NPH3 domain and has received little attention to date. However, considering that about one third of the 33 members of the NRL protein family are devoid of a CC domain[17], while the LIP motif is highly conserved (Supplementary Fig. 2d), LIP-mediated self-association with low affinity might be a functionally significant feature. This is supported by the – exclusively LIP-mediated - trimer formation of NPH3ΔC104 predicted by AF2M (Supplementary Fig. 2e).

Since NPH3 homo-oligomerization is mediated by a bipartite structured motif, we examined whether its individual parts serve distinct functions. Self-association linked to relocation appears to be a unique feature of the CC domain and could potentially alter the subcellular

localization of cytosolic NRLs through heteromeric complex formation with a PM-associated member. The second molecular function of the bipartite motif relates to PM association of NPH3. Here, we clearly demonstrated that homo-oligomerization of NPH3 in addition to its electrostatic interaction with phospholipids[11] is essential for PM recruitment (Fig. 3b, c). A comparable scenario has been described for other membrane-associated proteins such as the nanodomain-organizing REMORIN[41] or the 'helper' immune receptor NRG1.1[42]. In the context of PM attachment, the two parts obviously have an unequally redundant function. While the CC domain mediates strong PM association, the LIP allows weak PM binding when the CC domain is destabilized (NPH3_WLM/E, Fig. 3b, c).

Thirdly, the C-terminal bipartite self-association motif contributes to the higher-order oligomeric states of phase-separated NPH3 (NPH3ΔLIP_WLM/E, NPH3ΔC164, Fig. 3b; Fig. 4a). Notably, only the LIP motif (low affinity) is of importance here and acts cooperatively with the N-terminal BTB domain (weak interaction) in condensate formation (Fig. 4a), consistent with the finding that membrane-less assemblies can be formed by an ensemble of low-affinity molecular interactions[43]. Since interaction partners of NPH3 that are essential for condensate formation have not yet been identified[12] (own unpublished results), we suspected NPH3 to form a single-component condensate. Consequently, LIP-mediated self-association of NPH3 at the PM appears to be coupled to weak BTB-mediated homo-oligomerization in the cytosol, facilitating the formation of higher-order complexes. According to the AF2M prediction, the BTB domain (NPH3ΔC164 without the bipartite C-terminal motif) may be capable of antiparallel dimerization (Fig. 4b), enabling the assembly of cross-linked NPH3 trimers and ultimately a network of polymerized trimers in the cytosol (Supplementary Fig. 4d, e). In the rather 2D plane of the PM, formation of such a 3D polymer is, however, impossible due to steric constraints. Altogether, we propose a bistable switch of NPH3 controlled by subcellular localization. Here, a strict C-terminal trimerization at the PM is converted into a co-operative bivalent (LIP and BTB) homo-oligomerization in the cytosol.

During eukaryotic evolution, BTB domains progressively adapted to fulfill diverse cellular functions[26,27]. NRL family members are plant-specific BTB domain proteins and feature a conserved extension at the C-terminus of the BTB domain (α6 - α8)[36], which is crucial for condensate assembly of NPH3 (Fig. 4c). In addition, the NRL BTB domains adopted an N-terminal extension[36] with high structural variability among NRL family members. These variations could affect the ability, strength and orientation of BTB homo-oligomerization. It is worth noting that NPH3 may form part of a CULLIN3 RING E3 UBIQUITIN LIGASE (CRL3)[44]. Several – non NRL - plant BTB domain proteins act as substrate adapters in CRL3s with the BTB domain responsible for binding to the scaffold CULLIN3 (CUL3)[45]. Obligate BTB dimerization by apposition of two monomers in the same orientation is important for the function of many CRL3 orthologues in humans/yeast[36]. Such BTB dimer formation is unlikely

for NPH3[36] (Supplementary Fig. 1a) and furthermore, CUL3 was not identified as an NPH3 interaction partner in transgenic plants[12] (own unpublished data). Clearly, further biochemical work is needed to elucidate the possible involvement of NRL BTB domains in protein ubiquitylation. Variations in the N-terminal extension of NRL BTB domains could furthermore impact on homo-oligomerization of NRLs in general (CC/LIP vs. BTB). NRL family members lacking a stringent CC domain might therefore rely either on the BTB domain or the LIP motif for homo-oligomerization, depending on their respective affinities. In this context, NPY8/NRL5 which localizes close to the PM and belongs to a different NRL clade, was recently described to homomerize via its BTB domain based on *in vitro* pull-down assays[34]. Conversely, both the homo-oligomerization of NPH3 at the PM (Fig. 1c) and its interaction with RPT2 (Fig. 6b) occurs independently of its BTB domain *in planta*. Interestingly, AF2M predicts NPY8 to form either a BTB-mediated dimer or alternatively a LIP-mediated trimer. It is therefore of importance to validate these scenarios experimentally, taking into account potential changes in subcellular localization.

The use of biomolecular condensates as a means of spatial and temporal regulation is a ubiquitous phenomenon observed in all kingdoms of life. Plant biomolecular condensates are increasingly recognized as playing important roles in plant development and environmental responses. Prominent examples encompass flowering, auxin signaling, seed germination, RNA processing and immunity[26,27]. Reversible protein assemblies are usually drivers of either recruitment or sequestration. Sequestration of the auxin response factor ARF19 into cytosolic condensates regulates auxin transcriptional responses in a cell-specific manner by keeping the transcription factor away from the nucleus[46]. Regarding NPH3, transitioning into a condensed state likely sequesters the protein in the cytosol, thereby regulating its rate of reassociation with the PM, which can be observed not only upon retransfer to darkness[11] but also upon prolonged irradiation[13]. Mutations that disrupt NPH3 condensates almost completely abolished phototropic hypocotyl bending (Fig. 6a), suggesting that a precise dwell time of NPH3 in the cytosol is critical for function. However, we cannot rule out the possibility that the limited function of these variants is due to loss of an essential interaction that requires the C-terminal extension of the BTB domain of NPH3. Such an *in vivo* interaction partner has, however, not yet been identified[12] (own unpublished results). Overall, our data suggest that phase separation provides a mechanism to regulate cycling of NPH3 between the PM and the cytosol, particularly temporally. The elucidation of a putative important function of NPH3 at the PM, which must be modified in a transient and temporally tightly controlled manner to trigger phototropic hypocotyl bending, represents a major challenge for future research.

Material and Methods

Plant materials, transformation and growth conditions

Seeds of *Arabidopsis thaliana* (ecotype Columbia-0 (Col-0), *nph3-7* (SALK_110039, Col-0 background)) were obtained from the Nottingham Arabidopsis Stock Centre, and the transgenic lines expressing GFP-NPH3 under the control of 35S promoter in the *nph3-7* background have been described recently[11]. Stable transformation of *nph3-7* followed standard procedures.

Unless otherwise stated, seeds were surface sterilized and plated on solid half-strength Murashige and Skoog (MS) medium (pH 5.8) containing 1 % sucrose (w/v). Following stratification in the dark for 48-72 h at 4°C, seeds were exposed to fluorescent white light for 4 h. Seedlings were then grown in darkness for 68 h at 20°C. Subsequently, the etiolated seedlings were either kept in darkness or irradiated with BL (overhead BL (1 μmol $m^{-2}s^{-1}$) for up to 1 hour or, alternatively, GFP-laser treatment (488 nm) for up to 11 min during confocal observation of hypocotyl cells, as specified in the Figure legends). Independent experiments were carried out at least in triplicates. Representative images are presented.

Agrobacterium-mediated transient transformation of 3-4 weeks old *Nicotiana benthamiana* plants was performed as described previously[47]. *Agrobacterium tumefaciens* strain GV3101, transformed with a binary vector of interest, was resuspended in infiltration solution (10 mM MES [pH 5.6], 10 mM $MgCl_2$, 150 µM acetosyringone) at an OD_{600} of 0.1 – 0.2 and syringe-infiltrated into the abaxial epidermis of *N. benthamiana* leaves. For co-transformation, a 1:1 mixture was used, sometimes combined with co-introduction (by agroinfiltration of 35S::P19[48], OD_{600}: 0.01 – 0.05). Freshly transformed tobacco plants were kept under constant light for 24 h, subsequently transferred to darkness for 17 h (dark adaptation) and finally either kept in darkness (D) or irradiated [overhead BL (10 μmol $m^{-2}s^{-1}$) for up to 1 hour or, alternatively, the GFP-laser treatment (488 nm) for up to 11 min during confocal inspection of abaxial leaf epidermis cells, as specified in the Figure legends. Independent experiments were carried out at least in triplicates. Representative images are presented.

Cloning procedures

Cloning of N-terminally fluorophore-tagged NPH3 variants (GFP and/or RFP) into the destination vectors pB7WGR2 and/or pH7WGF2[49] for stable transformation or transient overexpression followed standard GATEWAY™ procedures. The 35S-driven NPH3 variants GFP/RFP:NPH3, GFP/RFP:NPH3_S744A, GFP/RFP:NPH3ΔC51 and GFP/RFP:NPH3_4K/A transformation vectors have been described before[11]. Transgenic plants were selected based on the hygromycin resistance conferred by pH7WGF2 and homozygous lines were established.

Site-directed mutagenesis was performed by PCR, while deletions were generated by primer extension PCR. PCR products and products of mutagenesis were verified by sequencing. A complete list of oligonucleotides used in this study for PCR is provided in Supplementary Table 1.

Expression and purification of proteins

For bacterial expression of the Arabidopsis C-terminal NPH3 variants N-terminally tagged with $(His)_6$-Maltose Binding Protein (MBP), the corresponding cDNA was amplified by PCR and cloned into the expression vector pDEST-HisMBP (Addgene plasmid #11085) using standard GATEWAY™ procedures. Recombinant NPH3 proteins were expressed using *Escherichia coli* BL21(DE3) host strain. Transformed *E.coli* BL21(DE3) was grown in liquid 2 x yeast extract and tryptone (2YT) medium containing ampicillin (100 μg/ml) at 37°C until an OD_{600} of 0.6. Protein expression was induced by adding IPTG to a final concentration of 0.5 mM. Following overnight growth at 16°C, bacteria were harvested by centrifugation (4000 rpm, 30 min, 4 °C). The pellet was frozen in liquid nitrogen. Following thawing on ice the cells were resuspended in bacterial protein extraction reagent B-PER (5 ml/g fresh weight) (Thermo Scientific, Waltham, USA) supplemented with Protease Inhibitor Mix-B (Serva, Heidelberg, Germany). Purification under native conditions was done by using the cleared BL21(DE3) lysate and Ni^{2+}-NTA agarose (Qiagen, Hilden, Germany) according to the manufacturer's protocol.

Size Exclusion Chromatography (SEC)

SEC was performed using the Superdex 200 Increase 10/300 GL column in combination with the ÄKTA™ pure chromatography system (Cytiva, Marlborough, USA). 200 µl of purified recombinant protein (approx. 2 mg/ml) was loaded onto the PBS-equilibrated (10 mM phosphate buffer, 140 mM NaCl, pH 7.4) column using a flow rate of 0.1 ml/min (UNICORN™ 7.0 program, Cytiva), and collected in 0.5 ml fractions using a 96-well fraction collector (Biozym, Oldendorf, Germany). The collected fractions were subjected to immunoblot analysis. The molecular weight of the recombinant NPH3 proteins was calibrated using standard size protein markers (High Molecular Weight Gel Filtration Calibration Kit, Cytiva): thyroglobulin (669 kDa, 5 mg/ml), Ferritin (440 kDa, 0.3 mg/ml), Aldolase (158 kDa, 4 mg/ml), Conalbumin (75 kDa, 3 mg/ml), Albumin (44 kDa, 4 mg/ml) and Chymotrypsinogen A (25 kDa, 3 mg/ml).

Preparation of microsomal membranes

Microsomal membrane fractions were prepared from transiently transformed and dark-adapted *N. benthamiana* leaves. Tissue was homogenized with 3 ml of ice-cold

homogenization buffer per g fresh weight (50 mM Hepes, pH 7.8, 500 mM sucrose, 1 % PVP-40, 3 mM dithiothreitol (DTT), 3 mM EDTA, supplemented with Complete Protease Inhibitor Mixture (Roche, Basel, Switzerland) and Phosphatase Inhibitor Mix 1 (Serva)). The homogenate was centrifuged at 10,000 × g for 20 min at 4°C. The supernatant was filtered through MiraCloth and subsequently centrifuged at 100,000 × g for 45 min at 4°C. The microsomal pellet was resuspended in ice-cold 5 mM Tris/MES, pH 6.5, 330 mM sucrose, 2 mM DTT, supplemented with Complete Protease Inhibitor Mixture (Roche) and Phosphatase Inhibitor Mix 1 (Serva). All the above steps were performed under red safe light conditions.

Co-Immunoprecipitation (CoIP)

In vivo interaction of fluorophore-tagged NPH3 variants was tested by using total plant protein extracts obtained from transiently transformed *N. benthamiana* leaves according to [50] with slight modifications. Dark-adapted tobacco plants were either kept in darkness or treated with overhead BL (10 μmol $m^{-2}s^{-1}$) for 1 h. Approximately 500 mg of leaf tissue was ground thoroughly under red safe light illumination and suspended in solubilization buffer (50 mM Tris, pH 7.5, 150 mM NaCl, 1 mM EDTA, 0.75% Triton X-100 supplemented with Complete Protease Inhibitor Mixture (Roche) and Phosphatase Inhibitor Mix 1 (Serva)). After 1 h incubation on an overhead rotor at 4 °C, cell debris-removed supernatant was incubated with equilibrated 20 μl GFP-Trap® or RFP-Trap® agarose beads (ChromoTek and Proteintech Company, Planegg-Martinsried, Germany) for 1 h in the cold room with overhead rotation. The beads were washed three times with solubilization buffer containing 0.1% Triton X-100, followed by a final washing step using 50 mM Tris, pH 7.5, 150 mM NaCl. Finally, proteins were eluted by adding 40 µl of 2 × SDS sample buffer (100 mM Tris-HCl pH 6.8, 20% glycerol, 2% β-Mercaptoethanol, 4% SDS, 0.02% bromophenol blue) and boiling at 95 °C for 10 min. The denatured proteins were subsequently separated by SDS-PAGE.

Protein quantification, SDS-PAGE and Western Blotting

Protein concentration was determined using ROTI® Nanoquant (Carl Roth, Karlsruhe, Germany) according to the manufacturer's protocol.

SDS-PAGE, Western blotting and immunodetection followed standard procedures. Total proteins were extracted from transiently transformed *N. benthamiana* leaves (2 leaf discs) by directly grinding in 100 μl 2 × SDS sample buffer under red safe light illumination. Proteins were denatured by incubation at 95°C for 5 min.

Chemiluminescence was detected using an Amersham ImageQuant 800 (Cytiva) system. Images were processed with Adobe Photoshop CS5 (Adobe Inc., San José, CA, USA) for adjustment of brightness and contrast. Chemiluminescence detection was performed using the ECL™ Prime Western Blot Detection Reagent (Cytiva).

The following antibodies were used in this study: anti-NPH3-S744P[11] (1:500), anti-NPH3[11] (1:1000) , anti-GFP (1:1000, Thermo Scientific, catalog number: A-11122, lot: 2477546), anti-RFP 5F8 (1:1000, ChromoTek and Proteintech Company, catalog number: 5f8-150, lot: 104272-05), anti-His_6 (1:2000, Roche/Merck, Darmstadt, Germany, catalog no: 11965085001).

Hypocotyl Phototropism analysis

Phototropism was performed using *A. thaliana* seedlings which were grown in the dark for 72 h on vertically oriented solid half-strength MS plates containing 1 % sucrose. Etiolated seedlings were then transferred to a LED chamber and illuminated with unilateral BL (1 μmol m^{-2} s^{-1}) for 24 h. Plates were scanned, and the inner hypocotyl angle was measured for each seedling using ImageJ[51]. The curvature angle was calculated as the difference between 180° and the measured value. For each transgenic line three biological replicates ($n \geq 30$ seedlings per experiment) were performed, alongside with the appropriate controls (Col-0, *nph3-7*).

AlphaFold Predictions

To predict protein and protein complex structures we used the AlphaFold2-Multimer program developed by Google DeepMind[31,32] through a subscription to the Google Colab v1.5.5[52] (https://colab.research.google.com/github/sokrypton/ColabFold/blob/main/AlphaFold2.ipynb) following guidelines on the document. As an alternative, AF3 predictions (developed by Google DeepMind and Isomorphic Labs)[33] were generated via the newly launched AlphaFold server (https://golgi.sandbox.google.com/about). Where indicated, predictions are colored according to the AF2 produced per-residue confidence metric called the local distance difference test (pLDDT)[32,53]. Models were colored in PyMol (The PyMOL Molecular Graphics System, Version 2.5.8 Schrödinger, LLC).

Confocal microscopy

Live-cell imaging was performed using the Leica TCS SP8 (upright) confocal laser scanning microscope. Imaging was done by using a 63x/1.20 water immersion objective. For excitation and emission of fluorophores, the following laser settings were used: GFP, excitation 488 nm, emission 505-530 nm; RFP, excitation 558 nm, emission 600-630 nm. All CLSM images in a single experiment were captured with the same settings using the Leica Confocal Software. For simultaneous imaging of samples expressing two fluorophores, sequential scanning mode was used supported by Leica Confocal Software. All experiments were repeated at least three times. Both the focal plane images and Z-stack maximum projection images were processed using Leica Application Suite X 3.7.4.23463.

Data analysis

For all quantitative CoIPs, the protein band intensities of GFP and RFP from IP:GFP were determined by Western blot quantification using ImageJ software as described by Hossein Davarinejad (http://www.yorku.ca/yisheng/Internal/Protocols/ImageJ.pdf). As a next step, the ratio of RFP band intensity to the corresponding GFP band intensity was determined. The values given in Fig. 2b were normalized to NPH3WT/NPH3ΔC104 (dark; left panel) and NPH3_WLM/E/NPH3ΔC51 (dark; right panel). Likewise, the values in Supplementary Fig. 2b were normalized to NPH3ΔC51/NPH3ΔC104 (dark).
The angles of phototropic curvature of all analyzed Arabidopsis genotypes (≥ 30 seedlings per genotype per replicate) were measured using ImageJ software. Graphical analysis was performed using the software GraphPad Prism. Statistical significance of the data was assessed using one-way ANOVA followed by *post hoc* Tukey multiple comparison test ($P < 0.05$). Error bars represent SD.

Supplementary Table 1:

List of primers used in this study

Mutagenesis primers	
NPH3_L_{592}E/V_{596}A_F	AACGAGAGGTTGCCAgaGAGAGTGGTGGcTCAAGTTCTCTTCTC
NPH3_L_{592}E/V_{596}A_R	GAGAAGAGAACTTGAgCCACCACTCTCtcTGGCAACCTCTCGTT
NPH3_V_{596}A/L_{599}E/Q_{603}A_F	GTGGTGGcTCAAGTTgaaTTCTCGGAGgcAGTCAAGATCAGCAA
NPH3_V_{596}A/L_{599}E/Q_{603}A_R	TTGCTGATCTTGACTgcCTCCGAGAAttcAACTTGAgCCACCAC
NPH3_L_{664}E _F	AACACGTTGAAGTTCGAGgaAGAGACGGTGAAGACCAAG
NPH3_ L_{664}E _R	CTTGGTCTTCACCGTCTCTtcCTCGAACTTCAACGTGTT
NPH3_M_{681}E_F	CAGAACGAGATGGAAGTGgaGCAACGACAGTTTGAGAAG
NPH3_M_{681}E_R	CTTCTCAAACTGTCGTTGCtcCACTTCCATCTCGTTCTG
NPH3_W_{650}E_F	CAATCGTTTCAGGAAGGAgaGGCTGCAGCCAAGAAGGAT
NPH3_W_{650}E_R	ATCCTTCTTGGCTGCAGCCtcTCCTTCCTGAAACGATTG
Primer extension PCR (deletion constructs)	
NPH3ΔLIP_F	CAGAACGAGAGGTTGCCATCGGAGCAAGTCAAGATC
NPH3ΔLIP_R	GATCTTGACTTGCTCCGATGGCAACCTCTCGTTCTG
NPH3ΔBTBα6-8_F	GTGGTTCTGTCTTCATGGAGTAATCCAAAAGGTATT
NPH3ΔBTBα6-8_R	AATACCTTTTGGATTACTCCATGAAGACAGAACCAC
NPH3ΔBTBα8_F	TGTGAAAAGCTCTCACCTAGTAATCCAAAAGGTATT
NPH3ΔBTBα8_R	AATACCTTTTGGATTACTAGGTGAGAGCTTTTCACA
GATEWAY	
NPH3_attB1_F	AAAAAGCAGGCTTAATGTGGGAATCTGAGAGCGAC
NPH3_attB2_R	AGAAAGCTGGGTGTCATGAAATTGAGTTCCTCCA

NPH3_S744A_attB2_R	Reuter *et al.*, 2021
NPH3ΔN197_attB1_F	AAAAAGCAGGCTTAATGAGTAATCCAAAAGGTATTAGA
NPH3ΔC51_attB2_R	Reuter *et al.*, 2021
NPH3ΔC104_attB2_R	AGAAAGCTGGGTGTCATGTTGCTTCGATCAATGTCTT
NPH3ΔC164_attB2_R	AGAAAGCTGGGTGTCACATACATGCGTCCATTGATAG
NPH3-C104_attB1_F	AAAAAGCAGGCTTAATGCCACAATCGTTTCAGGAAGGA
RPT2_attB1_F	AAAAAGCAGGCTTAATGGCAACAGAAGGAAAAAACCCCA
RPT2_attB2_R	AGAAAGCTGGGTGTTAAGAGATTGAGAATCTTCGTCTC
TOPO cloning	
NPH3-C51_F	CACCATGTCTTCTTCGGCTTGGACCAG

Acknowledgements

This work was supported by the German Research Foundation (DFG) with a grant to C.O. (CRC 1101-B09) and grants for scientific equipment (INST 37/819-1 FUGG, INST 37/991-1 FUGG). We are grateful to Nathalie Zgoda for data analysis and Franziska Lanz and Ricarda Furkert for their support in analyzing the recombinant C-terminal NPH3 fusion proteins. We further thank Chenlei Hua and Lisha Zhang for SEC support and Sandra Richter for SP8 support.

References

1 Christie, J. M. & Murphy, A. S. Shoot phototropism in higher plants: new light through old concepts. *Am. J. Bot.* **100**, 35-46 (2013).
2 Fankhauser, C. & Christie, J. M. Plant phototropic growth. *Curr. Biol.* **25**, R384-389 (2015).
3 Legris, M. & Boccaccini, A. Stem phototropism toward blue and ultraviolet light. *Physiol. Plant* **169**, 357-368 (2020).
4 Küpers, J. J., Oskam, L. & Pierik, R. Photoreceptors Regulate Plant Developmental Plasticity through Auxin. *Plants (Basel)* **9** (2020).
5 Haga, K. & Sakai, T. Photosensory adaptation mechanisms in hypocotyl phototropism: how plants recognize the direction of a light source. *J. Exp. Bot.* **74**, 1758-1769 (2023).
6 Willige, B. C. *et al.* D6PK AGCVIII kinases are required for auxin transport and phototropic hypocotyl bending in Arabidopsis. *Plant Cell* **25**, 1674-1688 (2013).
7 Zourelidou, M. *et al.* Auxin efflux by PIN-FORMED proteins is activated by two different protein kinases, D6 PROTEIN KINASE and PINOID. *Elife* **3** (2014).
8 Ding, Z. *et al.* Light-mediated polarization of the PIN3 auxin transporter for the phototropic response in Arabidopsis. *Nat. Cell. Biol.* **13**, 447-452 (2011).
9 Zhang, Y. *et al.* Clathrin regulates blue light-triggered lateral auxin distribution and hypocotyl phototropism in Arabidopsis. *Plant Cell Environ.* **40**, 165-176 (2017).
10 Hohm, T., Preuten, T. & Fankhauser, C. Phototropism: translating light into directional growth. *Am. J. Bot.* **100**, 47-59 (2013).
11 Reuter, L. *et al.* Light-triggered and phosphorylation-dependent 14-3-3 association with NON-PHOTOTROPIC HYPOCOTYL 3 is required for hypocotyl phototropism. *Nat. Comm.* **12**, 6128 (2021).
12 Sullivan, S. *et al.* Regulation of plant phototropic growth by NPH3/RPT2-like substrate phosphorylation and 14-3-3 binding. *Nat. Commun.* **12**, 6129 (2021).

13 Haga, K., Tsuchida-Mayama, T., Yamada, M. & Sakai, T. Arabidopsis ROOT PHOTOTROPISM2 Contributes to the Adaptation to High-Intensity Light in Phototropic Responses. *Plant Cell* **27**, 1098-1112 (2015).
14 Sullivan, S., Kharshiing, E., Laird, J., Sakai, T. & Christie, J. M. Deetiolation Enhances Phototropism by Modulating NON-PHOTOTROPIC HYPOCOTYL3 Phosphorylation Status. *Plant Physiol.* **180**, 1119-1131 (2019).
15 Motchoulski, A. & Liscum, E. *Arabidopsis* NPH3: A NPH1 Photoreceptor-Interacting Protein Essential for Phototropism. *Science* **286**, 961-964 (1999).
16 Haga, K., Takano, M., Neumann, R. & Iino, M. The Rice COLEOPTILE PHOTOTROPISM1 gene encoding an ortholog of Arabidopsis NPH3 is required for phototropism of coleoptiles and lateral translocation of auxin. *Plant Cell* **17**, 103-115 (2005).
17 Pedmale, U. V., Celaya, R. B. & Liscum, E. in *Arabidopsis Book* Vol. 8 e0125 (2010).
18 Christie, J. M., Suetsugu, N., Sullivan, S. & Wada, M. Shining Light on the Function of NPH3/RPT2-Like Proteins in Phototropin Signaling. *Plant Physiol.* **176**, 1015-1024 (2018).
19 Treml, B. S. *et al.* The gene ENHANCER OF PINOID controls cotyledon development in the Arabidopsis embryo. *Development* **132**, 4063-4074 (2005).
20 Cheng, Y., Qin, G., Dai, X. & Zhao, Y. NPY1, a BTB-NPH3-like protein, plays a critical role in auxin-regulated organogenesis in Arabidopsis. *Proc. Natl. Acad. Sci. U S A* **104**, 18825-18829 (2007).
21 Furutani, M. *et al.* The gene MACCHI-BOU 4/ENHANCER OF PINOID encodes a NPH3-like protein and reveals similarities between organogenesis and phototropism at the molecular level. *Development* **134**, 3849-3859 (2007).
22 Li, Y., Dai, X., Cheng, Y. & Zhao, Y. NPY genes play an essential role in root gravitropic responses in Arabidopsis. *Mol. Plant* **4**, 171-179 (2011).
23 Glanc, M. *et al.* AGC kinases and MAB4/MEL proteins maintain PIN polarity by limiting lateral diffusion in plant cells. *Curr. Biol.* (2021).
24 Waksman, T. *et al.* Phototropin phosphorylation of ROOT PHOTOTROPISM 2 and its role in mediating phototropism, leaf positioning, and chloroplast accumulation movement in Arabidopsis. *Plant J.* **114**, 390-402 (2023).
25 Furutani, M. *et al.* Polar-localized NPH3-like proteins regulate polarity and endocytosis of PIN-FORMED auxin efflux carriers. *Development* **138**, 2069-2078 (2011).
26 Emenecker, R. J., Holehouse, A. S. & Strader, L. C. Biological Phase Separation and Biomolecular Condensates in Plants. *Annu. Rev. Plant Biol.* **72**, 17-46 (2021).
27 Field, S., Jang, G.-J., Dean, C., Strader, L. C. & Rhee, S. Y. Plants use molecular mechanisms mediated by biomolecular condensates to integrate environmental cues with development. *The Plant Cell* **35**, 3173-3186 (2023).
28 Shin, Y. & Brangwynne, C. P. Liquid phase condensation in cell physiology and disease. *Science* **357** (2017).
29 Banani, S. F., Lee, H. O., Hyman, A. A. & Rosen, M. K. Biomolecular condensates: organizers of cellular biochemistry. *Nat. Rev. Mol. Cell Biol.* **18**, 285-298 (2017).
30 Lyon, A. S., Peeples, W. B. & Rosen, M. K. A framework for understanding the functions of biomolecular condensates across scales. *Nat. Rev. Mol. Cell Biol.* **22**, 215-235 (2021).
31 Jumper, J. *et al.* Highly accurate protein structure prediction with AlphaFold. *Nature* **596**, 583-589 (2021).
32 Evans, R. *et al.* Protein complex prediction with AlphaFold-Multimer. *bioRxiv*, 2021.2010.2004.463034 (2022).
33 Abramson, J. *et al.* Accurate structure prediction of biomolecular interactions with AlphaFold 3. *Nature* (2024).
34 Upadhyay-Tiwari, N. *et al.* The Non-Phototrophic Hypocotyl3 (NPH3)-domain protein NRL5 is a trafficking-associated GTPase essential for drought resistance. *bioRxiv*, 2023.2005.2010.540297 (2023).

35 Inada, S., Ohgishi, M., Mayama, T., Okada, K. & Sakai, T. RPT2 is a signal transducer involved in phototropic response and stomatal opening by association with phototropin 1 in Arabidopsis thaliana. *Plant Cell* **16**, 887-896 (2004).
36 Bonchuk, A., Balagurov, K. & Georgiev, P. BTB domains: A structural view of evolution, multimerization, and protein-protein interactions. *Bioessays* **45**, e2200179 (2023).
37 Stogios, P. J., Downs, G. S., Jauhal, J. J., Nandra, S. K. & Privé, G. G. Sequence and structural analysis of BTB domain proteins. *Genome Biol.* **6**, R82 (2005).
38 Pedmale, U. V. & Liscum, E. Regulation of phototropic signaling in Arabidopsis via phosphorylation state changes in the phototropin 1-interacting protein NPH3. *J. Biol. Chem.* **282**, 19992-20001 (2007).
39 Tsuchida-Mayama, T. *et al.* Mapping of the phosphorylation sites on the phototropic signal transducer, NPH3. *Plant Sci* **174**, 626-633 (2008).
40 Kimura, T. *et al.* Phosphorylation of NONPHOTOTROPIC HYPOCOTYL3 affects photosensory adaptation during the phototropic response. *Plant Physiol.* (2021).
41 Martinez, D. *et al.* Coiled-coil oligomerization controls localization of the plasma membrane REMORINs. *J. Struct. Biol.* **206**, 12-19 (2019).
42 Jacob, P. *et al.* Plant "helper" immune receptors are $Ca^{(2+)}$-permeable nonselective cation channels. *Science* **373**, 420-425 (2021).
43 Boija, A. *et al.* Transcription Factors Activate Genes through the Phase-Separation Capacity of Their Activation Domains. *Cell* **175**, 1842-1855.e1816 (2018).
44 Roberts, D. *et al.* Modulation of Phototropic Responsiveness in Arabidopsis through Ubiquitination of Phototropin 1 by the CUL3-Ring E3 Ubiquitin Ligase CRL3NPH3 *The Plant Cell* **23**, 3627-3640 (2011).
45 Ban, Z. & Estelle, M. CUL3 E3 ligases in plant development and environmental response. *Nat. Plants* **7**, 6-16 (2021).
46 Powers, S. K. *et al.* Nucleo-cytoplasmic Partitioning of ARF Proteins Controls Auxin Responses in Arabidopsis thaliana. *Mol. Cell* **76**, 177-190.e175 (2019).
47 Blatt, M. R. & Grefen, C. Applications of fluorescent marker proteins in plant cell biology. *Methods Mol Biol.* **1062**, 487-507 (2014).
48 Win, J. & Kamoun, S. pCB301-p19: A Binary Plasmid Vector to Enhance Transient Expression of Transgenes by Agroinfiltration. http://www.KamounLab.net (2004).
49 Karimi, M., Depicker, A. & Hilson, P. Recombinational cloning with plant gateway vectors. *Plant Physiol.* **145**, 1144-1154 (2007).
50 Albert, I. *et al.* An RLP23–SOBIR1–BAK1 complex mediates NLP-triggered immunity. *Nat. Plants* **1**, 15140 (2015).
51 Schindelin, J. *et al.* Fiji: an open-source platform for biological-image analysis. *Nat. Methods* **9**, 676-682 (2012).
52 Mirdita, M. *et al.* ColabFold: making protein folding accessible to all. *Nat. Methods* **19**, 679-682 (2022).
53 Elfmann, C. & Stülke, J. PAE viewer: a webserver for the interactive visualization of the predicted aligned error for multimer structure predictions and crosslinks. *Nucleic Acids Res.* **51**, W404-W410 (2023).

Figures

Fig. 1: NPH3 self-associates at the PM and within cytosolic condensates independent of its BTB domain.

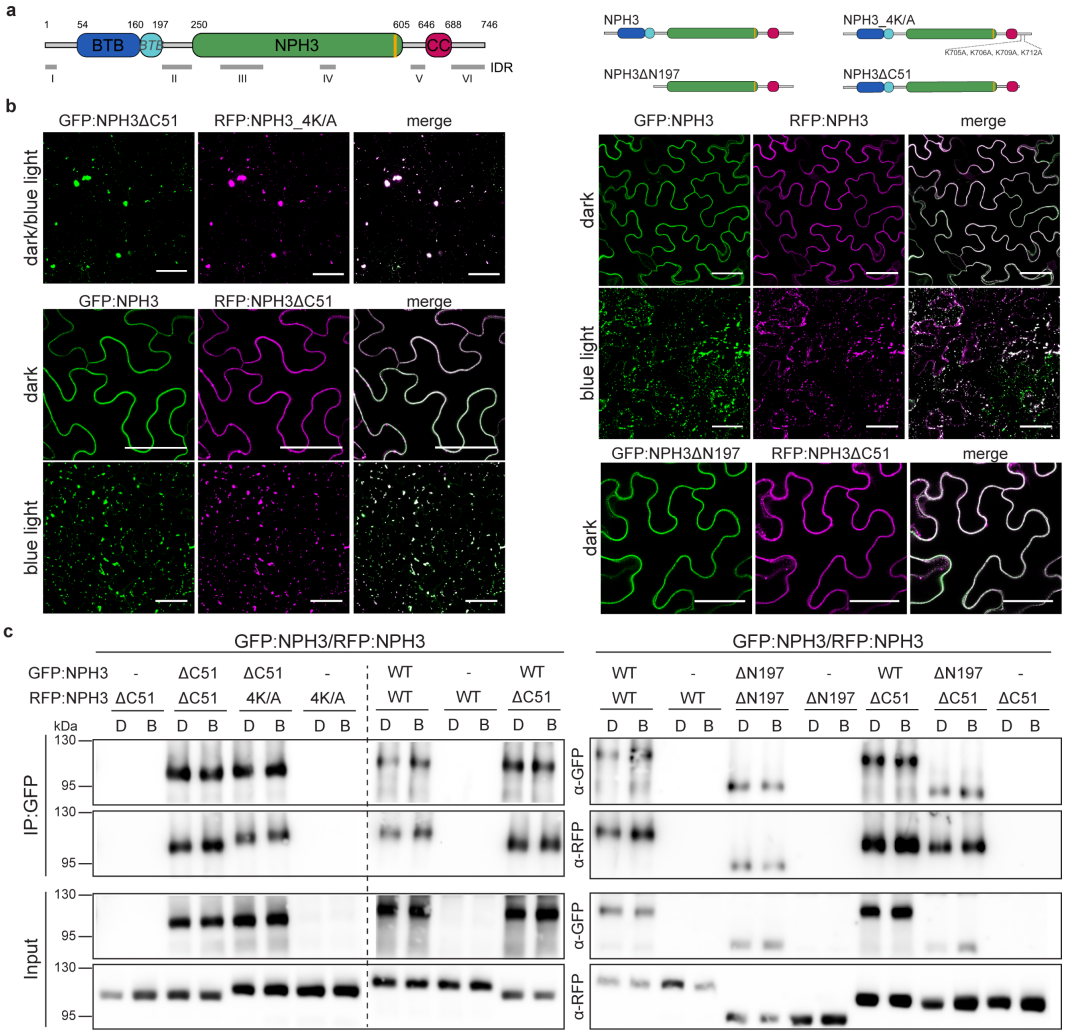

a Domain architecture of NPH3 (746 amino acids) and location of IDRs (AF2 prediction). C-terminal BTB extension highlighted in light blue (*BTB*), LIP motif highlighted in yellow, see text for details **(left panel).** Schematic representation of NPH3 constructs used **(right panel)**. **b** Representative confocal images of leaf epidermal cells from *N. benthamiana* transiently co-expressing different GFP/RFP:NPH3 variants. Expression was driven by the 35S promoter. Dark-adapted tobacco plants were either kept in darkness or treated with blue light (~ 11 min GFP laser). Z-stack projections of BL-treated samples are shown. Scale bars, 50 µm. These experiments were repeated at least three times with similar results. **c** *In vivo* interaction of GFP/RFP:NPH3 variants transiently co-expressed (35S promoter) in *N. benthamiana* leaves. Dark-adapted tobacco plants were either kept in darkness (D) or treated with blue light (B) (10 µmol $m^{-2}s^{-1}$) for 1 hour. The crude protein extract was immunoprecipitated using GFP beads. Input and immunoprecipitated (IP:GFP) proteins were separated on 10 % SDS-PAGE gels, followed by immunoblotting with anti-GFP and anti-RFP antibodies, respectively. Experiments were performed at least two times with similar results. Dotted lines indicate that the same blot has been sliced and the sides swapped. **See also Supplementary Fig 1.**

Supplementary Fig. 1: Self-association of NPH3 is independent of its subcellular localization.

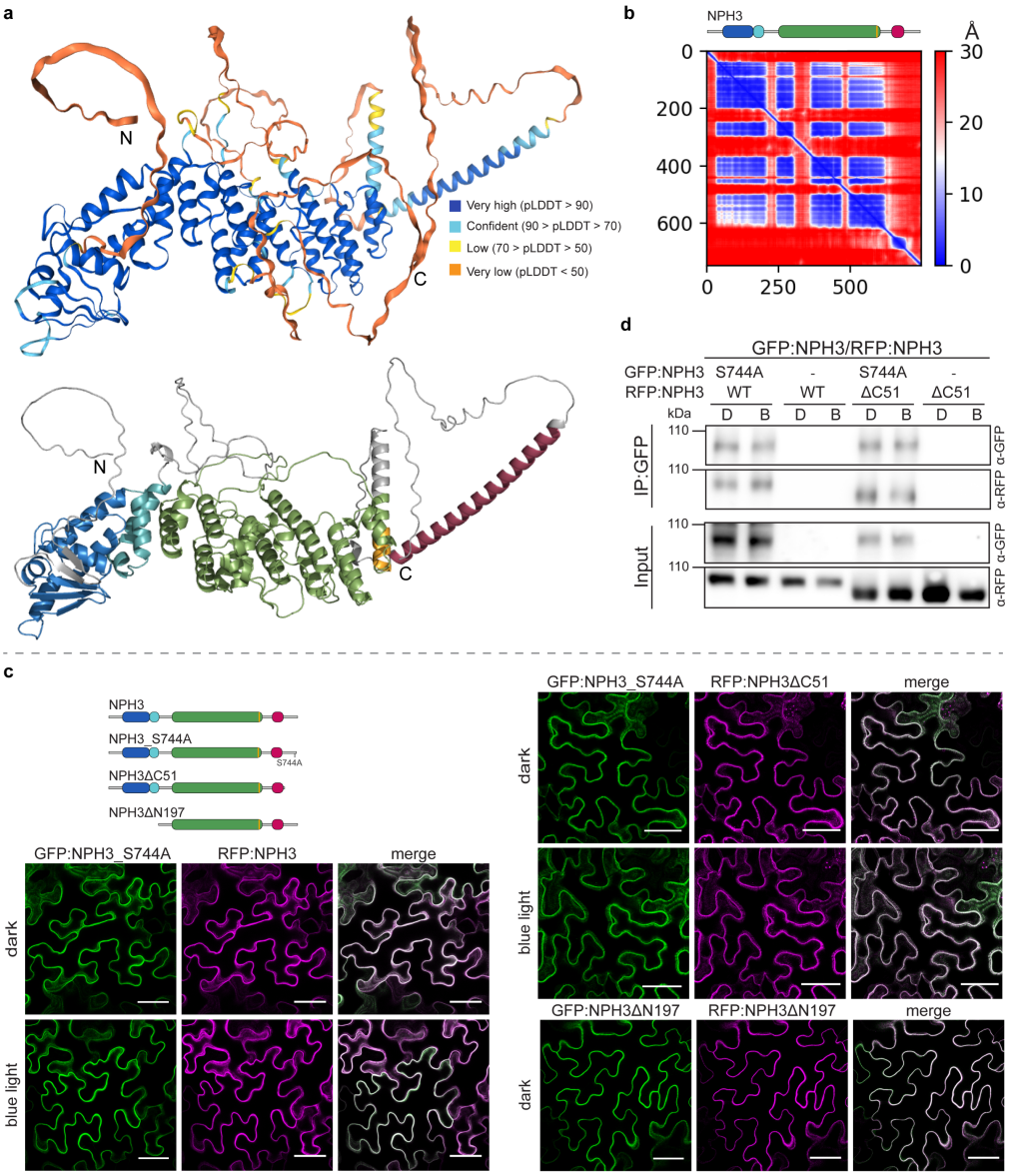

a Protein structure of NPH3 predicted by AF2. Color-coding of the ribbon plot is based either on the 'per residue confidence score' (pLDDT, **upper panel**) or on the schematic domain representation (Fig. 1a) (**lower panel**). N, N-terminus; C, C-terminus. **b** PAE plot of the NPH3 structure shown in (a). **c** Representative confocal images of leaf epidermal cells from *N. benthamiana* transiently co-expressing (35S promoter) different GFP/RFP:NPH3 variants. Dark-adapted tobacco plants were either kept in darkness or treated with blue light (~ 11 min GFP laser). Z-stack projections are shown, except for GFP:NPH3ΔN197/RFP:NPH3ΔN197. Scale bars, 50 µm. These experiments were repeated at least three times with similar results. **d** *In vivo* interaction of GFP/RFP:NPH3 variants transiently co-expressed (35S promoter) in *N. benthamiana* leaves. Dark-adapted tobacco plants were either kept in darkness (D) or treated with blue light (B) (10 µmol $m^{-2}s^{-1}$) for 1 hour. The crude protein extract was immunoprecipitated using GFP beads. Input and immunoprecipitated (IP:GFP) proteins were separated on 10 % SDS-PAGE gels, followed by immunoblotting with anti-GFP and anti-RFP antibodies, respectively. Experiments were performed at least two times with similar results.

Fig. 2: NPH3 is characterized by a bipartite C-terminal self-association motif.

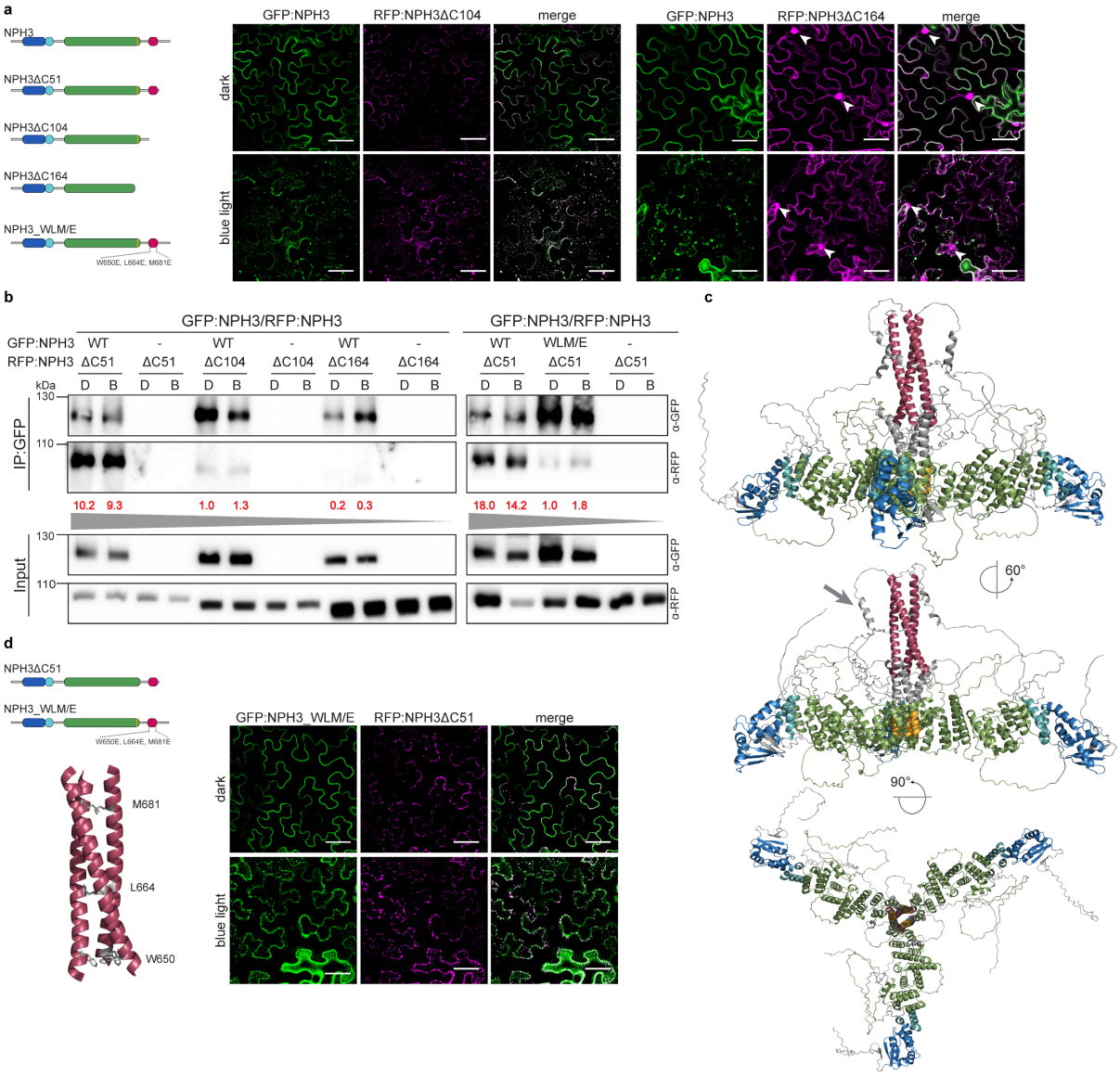

a Schematic representation of NPH3 variants used and representative confocal images of leaf epidermal cells from *N. benthamiana* transiently co-expressing (35S promoter) different GFP/RFP:NPH3 variants. Dark-adapted tobacco plants were either kept in darkness or treated with blue light (~ 11 min GFP laser). Z-stack projections of BL-treated samples are shown. Scale bars, 50 µm. The experiments were repeated at least three times with similar results. White arrowheads indicate nucleus. **b** *In vivo* interaction of GFP/RFP:NPH3 variants transiently co-expressed (35S promoter) in *N. benthamiana* leaves. Dark-adapted tobacco plants were either kept in darkness (D) or treated with blue light (B) (10 µmol $m^{-2}s^{-1}$) for 1 hour. The crude protein extract was immunoprecipitated using GFP beads. Input and immunoprecipitated proteins (IP:GFP) were separated on 10 % SDS-PAGE gels, followed by immunoblotting with anti-GFP and anti-RFP antibodies, respectively. Experiments were performed at least two times with similar results. Values in red represent the quantification of RFP band intensities normalized to the GFP band intensities (IP:GFP). **c** Ribbon plot of the NPH3 trimer predicted by AF2M and color-coded according to the schematic domain representation (Fig. 1a). Grey arrow: amphipathic helix. **d** Schematic representation of NPH3 variants used and enlarged view of the CC helix bundle showing the position of the mutated residues (**left panel**). Representative confocal images of leaf epidermal cells from *N. benthamiana* transiently co-expressing (35S promoter) different GFP/RFP:NPH3 variants

(**right panel**). Dark-adapted tobacco plants were either kept in darkness or treated with blue light (~ 11 min GFP laser). Z-stack projection of BL-treated sample is shown. Scale bars, 50 µm. The experiments were repeated at least three times with similar results. **See also Supplementary Fig 2.**

Supplementary Fig. 2: The bipartite C-terminal self-association motif of NPH3 consists of the CC domain and the LIP motif.

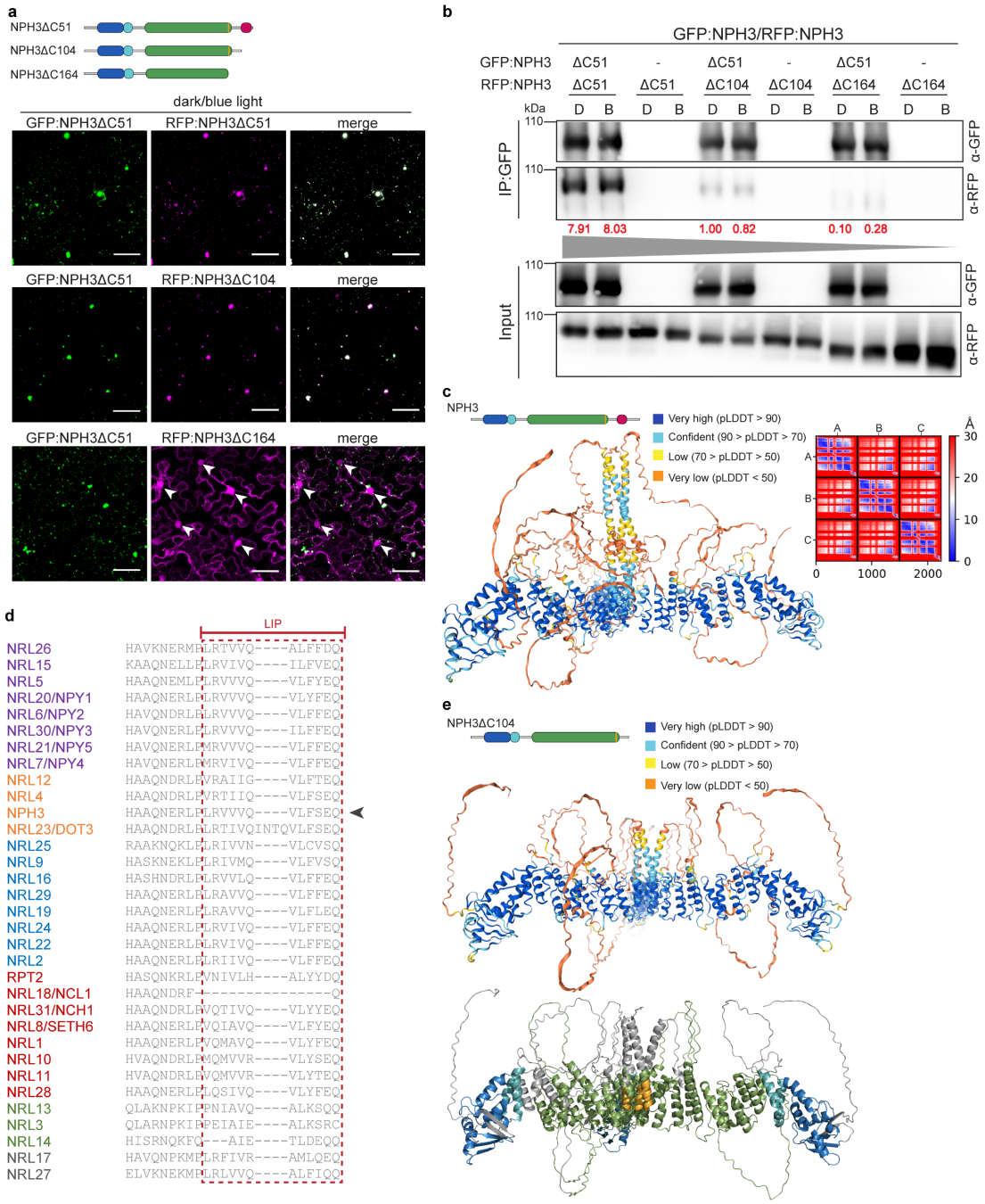

a Schematic representation of NPH3 variants used and representative confocal images of leaf epidermal cells from *N. benthamiana* transiently co-expressing (35S promoter) different GFP/RFP:NPH3 variants. Dark-adapted tobacco plants were either kept in darkness or treated with blue light (~ 11 min GFP laser). Z-stack projections are shown. Scale bars, 50 µm. Experiments were performed at least three times with similar results. White arrowheads indicate nucleus. **b** *In vivo* interaction of GFP/RFP:NPH3 variants transiently co-expressed (35S promoter) in *N. benthamiana* leaves. Dark-adapted tobacco plants were either kept in darkness (D) or treated with blue light (B) (10 µmol $m^{-2}s^{-1}$) for 1 hour. The crude protein extract was immunoprecipitated using GFP beads. Input and immunoprecipitated proteins (IP:GFP) were separated on 10 % SDS-PAGE gels, followed by immunoblotting with anti-GFP and anti-RFP antibodies, respectively. Experiments were performed at least three times

with similar results. Values in red represent quantification of RFP band intensities normalized to the GFP band (IP:GFP). **c** Ribbon plot of NPH3 trimer predicted by AF2M and color-coded according to the pLDDT score (**left panel**)**.** The corresponding PAE plot is shown in the **right panel**. **d** Amino acid alignment of the *Arabidopsis* NRL protein family focusing on the residues constituting the LIP motif in NPH3 (red dotted box). **e** Ribbon plot of the NPH3ΔC104 trimer predicted by AF2M and color-coded according to the pLDDT score (**upper panel**) or the schematic domain representation (Fig. 1a) (**lower panel**)**.**

Fig. 3: Homo-oligomerization mediated by the bipartite motif is essential for PM association of NPH3 *in vivo*.

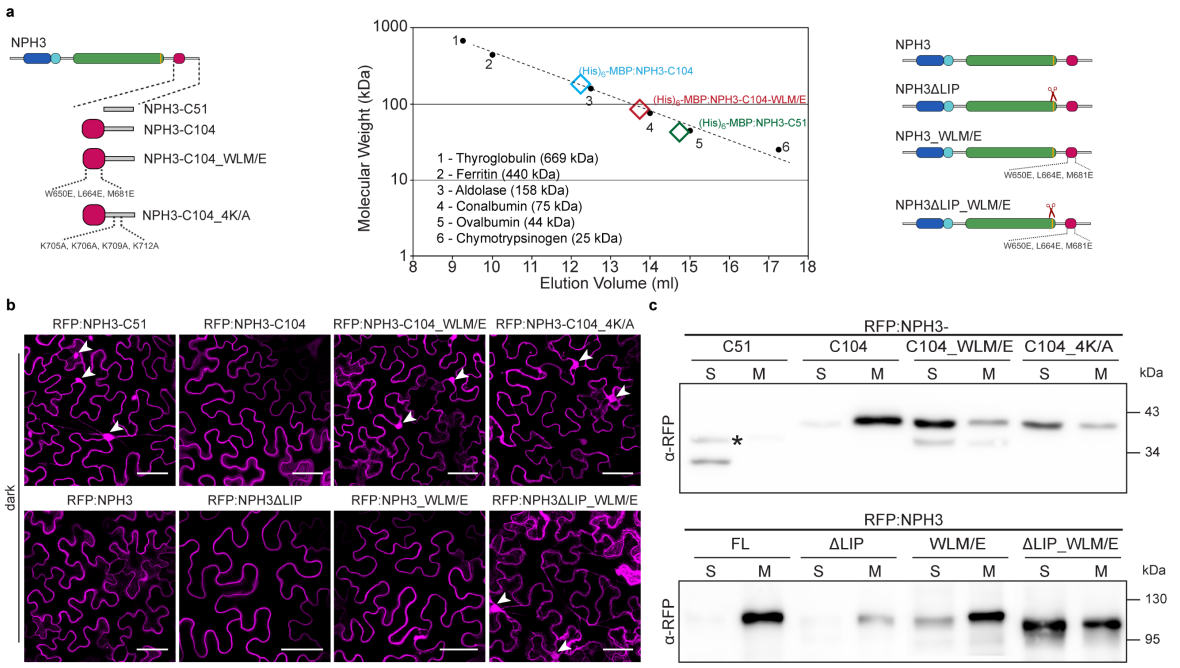

a Schematic representation of C-terminal NPH3 fragments **(left panel)** and NPH3 variants **(right panel)** used. Size Exclusion Chromatography **(middle panel)** of different NPH3 C-terminal fragments tagged with $(His)_6$-Maltose Binding Protein (MBP). Elution of molecular mass marker proteins (1-6) is indicated within the graph. Molecular weights of the proteins are given in logarithmic scale (Y-axis). **b** Representative confocal images of leaf epidermal cells from dark-adapted *N. benthamiana* transiently expressing (35S promoter) RFP:NPH3 variants. Z-stack projections are shown. Scale bars, 50 µm. White arrowheads indicate nucleus. **c** Representative α-RFP immunoblots following subcellular fractionation of protein extracts prepared from dark-adapted *N. benthamiana* leaves transiently expressing (35S promoter) RFP:NPH3 variants. Proteins in each fraction (~ 10 µg) were separated on 12% (NPH3 C-terminal fragments) or 10% (full-length NPH3 variants) SDS-PAGE gels. It is noteworthy that the total amount of soluble proteins (S) is ~10 times higher as compared to the total amount of microsomal proteins (M) after 100,000 × g centrifugation. (*) Asterisk indicates non-specific band. All experiments were performed at least three times with comparable results. **See also Supplementary Fig 3.**

Supplementary Fig. 3: Size Exclusion Chromatography (SEC) analysis of C-terminal NPH3 fragments.

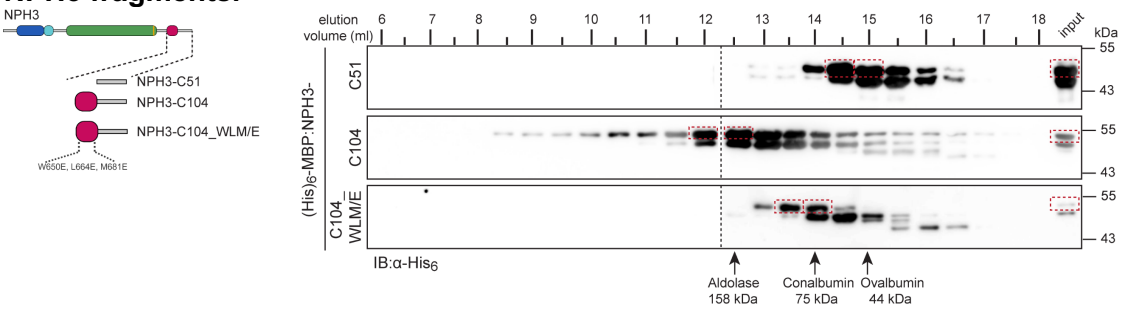

Schematic representation of C-terminal NPH3 fragments **(left panel)** and α-His immunological analysis of fractions obtained via size-exclusion chromatography of different purified NPH3 C-terminal fragments tagged with $(His)_6$-Maltose Binding Protein (MBP) (**right panel**). The red dotted boxes highlight the purified non-degraded fusion protein in the input as well as in the elution fractions. Arrows mark the elution peaks of the marker proteins with the indicated molecular mass.

Fig. 4: Condensate assembly of NPH3 requires the LIP motif and the BTB domain.

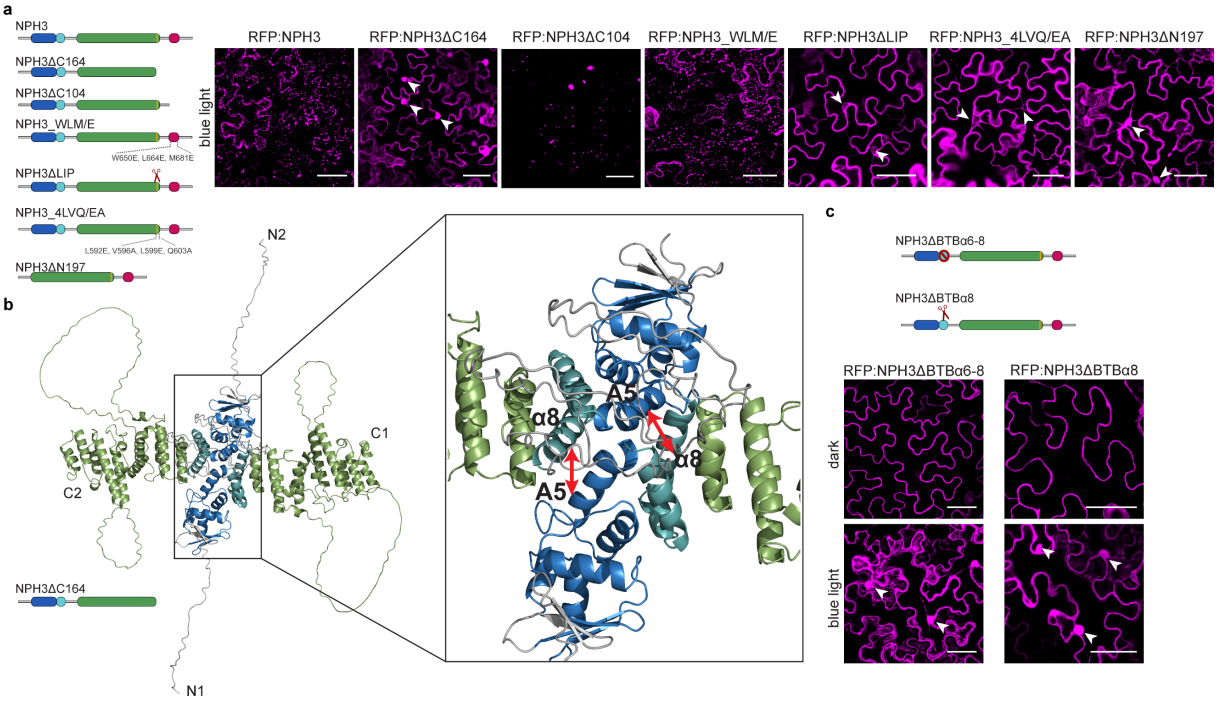

a Schematic representation of NPH3 variants used (LIP motif highlighted in yellow, see text for details) and representative confocal images of leaf epidermal cells from *N. benthamiana* transiently expressing (35S promoter) different RFP:NPH3 variants. Dark-adapted tobacco plants were treated with blue light (~ 11 min GFP laser). Z-stack projections are shown. Scale bars, 50 µm. White arrowheads indicate nucleus/cytoplasmic strands. **b** Ribbon plot of the NPH3ΔC164 dimer predicted by AF2M and color-coded according to the schematic domain representation (Fig. 1a). Enlarged view depicts the potential antiparallel BTB-BTB interaction based on the interaction between helix A5 of the core BTB (dark blue) and helix α8 of the C-terminal BTB extension (light blue). N1, N2, N-terminus; C1, C2, C-terminus. **c** Representative confocal images of leaf epidermal cells from *N. benthamiana* transiently expressing (35S promoter) RFP:NPH3 variants. Dark-adapted tobacco plants were either kept in darkness or treated with blue light (~ 11 min GFP laser). Z-stack projections of BL-treated samples are shown. Scale bars, 50 µm. White arrowheads indicate nucleus. All experiments were repeated at least three times with similar results. **See also Supplementary Fig 4.**

Supplementary Fig: 4: Crosslinking of NPH3 trimers via BTB-dependent antiparallel interactions could enable the formation of higher-order assemblies.

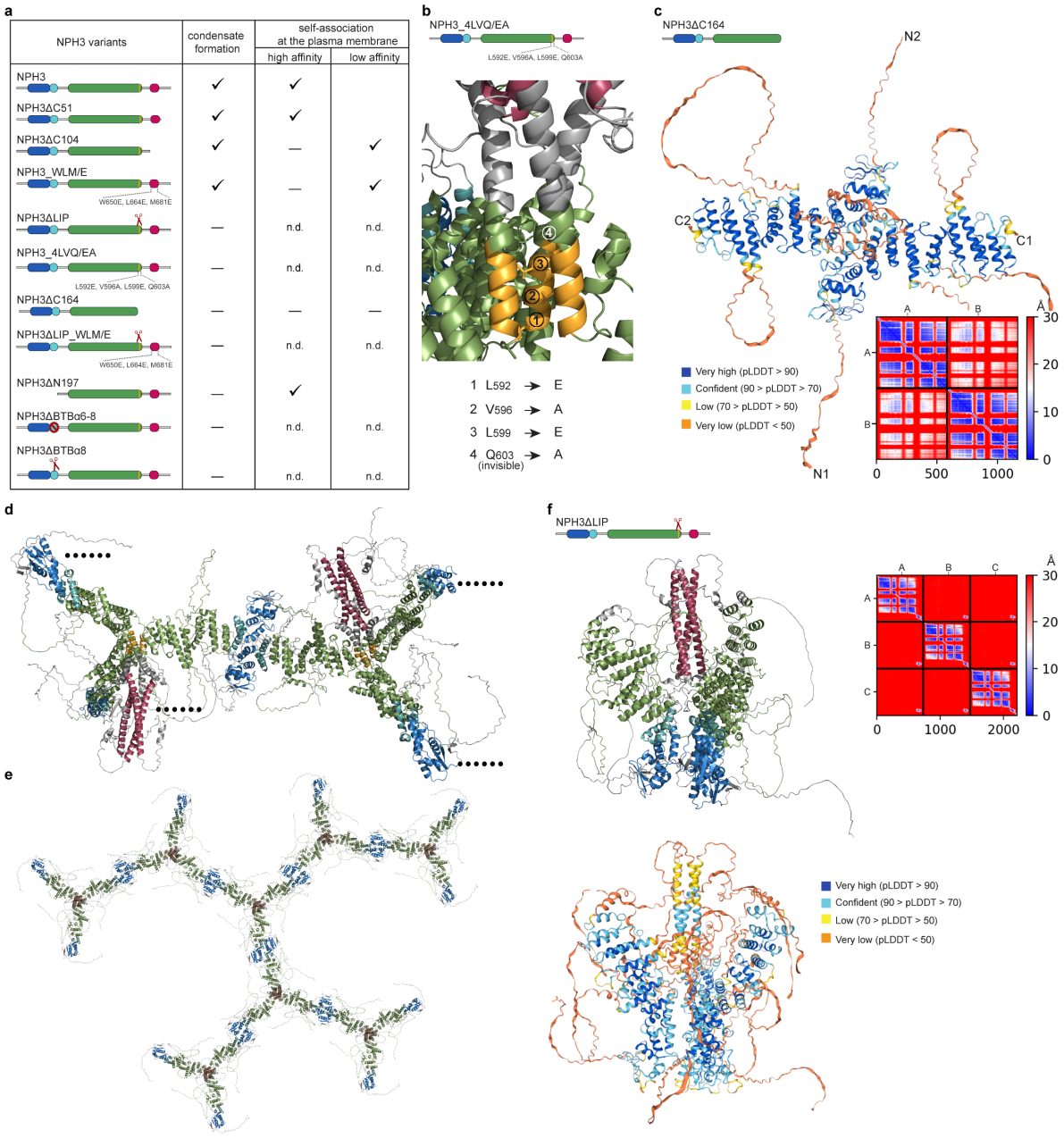

a Summary of NPH3 variants used and their molecular role in condensate formation and self-association at the plasma membrane. n.d., not determined. **b** Enlarged view of the LIP helix bundle showing the position of the mutated residues. **c** Ribbon plot of the NPH3ΔC164 dimer predicted by AF2M and color-coded according to the pLDDT score (**left panel**). The corresponding PAE plot is shown in the **right panel**. N1, N2, N-terminus; C1, C2, C-terminus. **d** Ribbon plot of two NPH3 trimers crosslinked via antiparallel BTB-BTB interaction. It should be noted that each trimer comprises two additional BTB domains that could be cross-linked. **e** Simplified illustration (based on the bottom view of a NPH3 trimer, see Fig. 2c lower panel) of NPH3 higher-order assemblies via antiparallel BTB-BTB interactions. **f** Ribbon plot of the NPH3ΔLIP trimer predicted by AF2M and color-coded according to the schematic domain representation (**upper panel left**) or the pLDDT score **(lower panel**). The corresponding PAE plot is shown in the **upper right panel**.

Fig. 5: Phot1-dependent dephosphorylation of NPH3 is independent of condensate formation and PM dissociation.

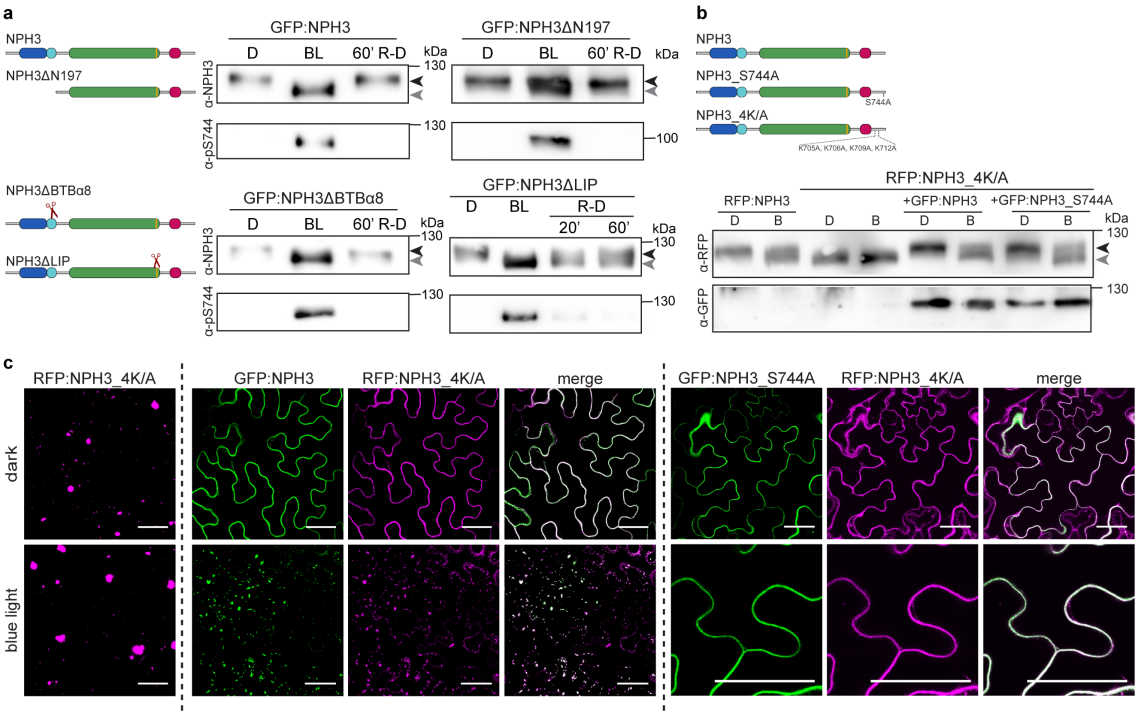

Black and grey arrowheads indicate the position of the phosphorylated and dephosphorylated NPH3 proteins, respectively. **a** Schematic representation of NPH3 variants used and immunoblot analysis of anti-GFP immunoprecipitates from *N. benthamiana* leaves transiently expressing (35S promoter) GFP:NPH3 variants. Dark-adapted tobacco plants were either maintained in darkness (D), treated with blue light (10 µmol $m^{-2}s^{-1}$) for 1 hour (BL) or re-transferred back to darkness for the indicated time after blue light irradiation (R-D). Immunoprecipitated proteins were separated on 7.5 % SDS-PAGE gels. **b** Schematic representation of NPH3 variants used and immunoblot analysis of total protein extracts from transiently transformed *N. benthamiana* co-expressing (35S promoter) RFP:NPH3_4K/A and GFP:NPH3 variants. Dark-adapted tobacco plants were either maintained in darkness (D) or treated with blue light (10 µmol $m^{-2}s^{-1}$) for 1 hour (B) and proteins were separated on a 7.5 % SDS-PAGE gel. **c** Representative confocal images of leaf epidermal cells from *N. benthamiana* transiently co-expressing (35S promoter) RFP:NPH3_4K/A either with GFP:NPH3 or GFP:NPH3_S744A. Dark-adapted tobacco plants were either kept in darkness or treated with blue light (~ 11 min GFP laser). Single expression of RFP:NPH3_4K/A is shown as control. Z-stack projections of the single expression of RFP:NPH3_4K/A and for the co-expression of GFP:NPH3/RFP:NPH3_4K/A (blue light-treated) are shown. Scale bars, 50 µm. All experiments were repeated at least three times with similar results.

Supplementary Fig. 5: Light-dependent changes in subcellular localization are retained in condensate-incompetent NPH3 variants.

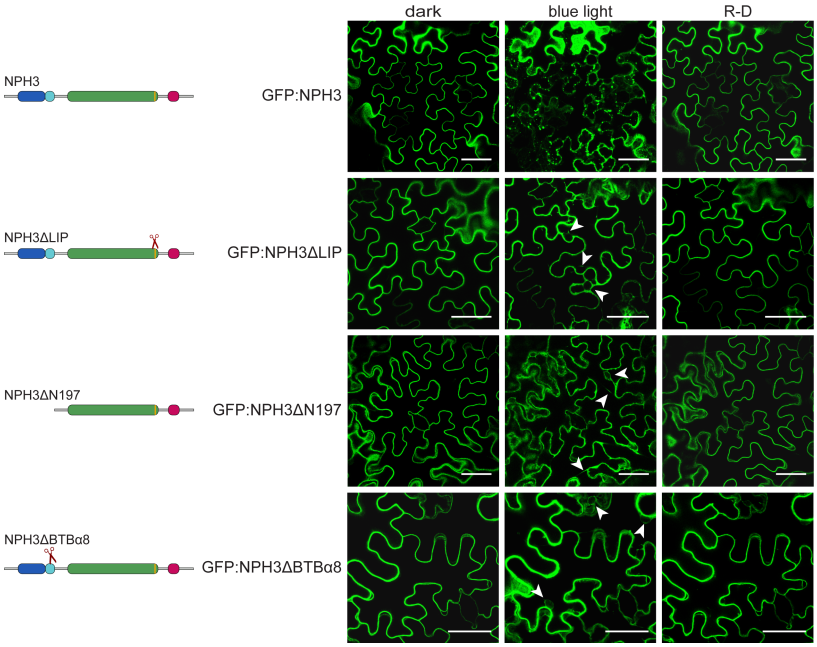

Schematic representation of NPH3 variants used and representative confocal images of leaf epidermal cells from *N. benthamiana* transiently expressing (35S promoter) different GFP:NPH3 variants. Dark-adapted tobacco plants were either maintained in darkness (dark), treated with blue light (~ 11 min GFP laser) or re-transferred back to darkness for 30 min after blue light irradiation (R-D). Z-stack projections of blue light treated samples are shown. Scale bars, 50 µm. Experiments were repeated at least three times with similar results. White arrowheads indicate cytoplasmic strands .

Fig. 6: Functional relevance of NPH3 condensate formation.

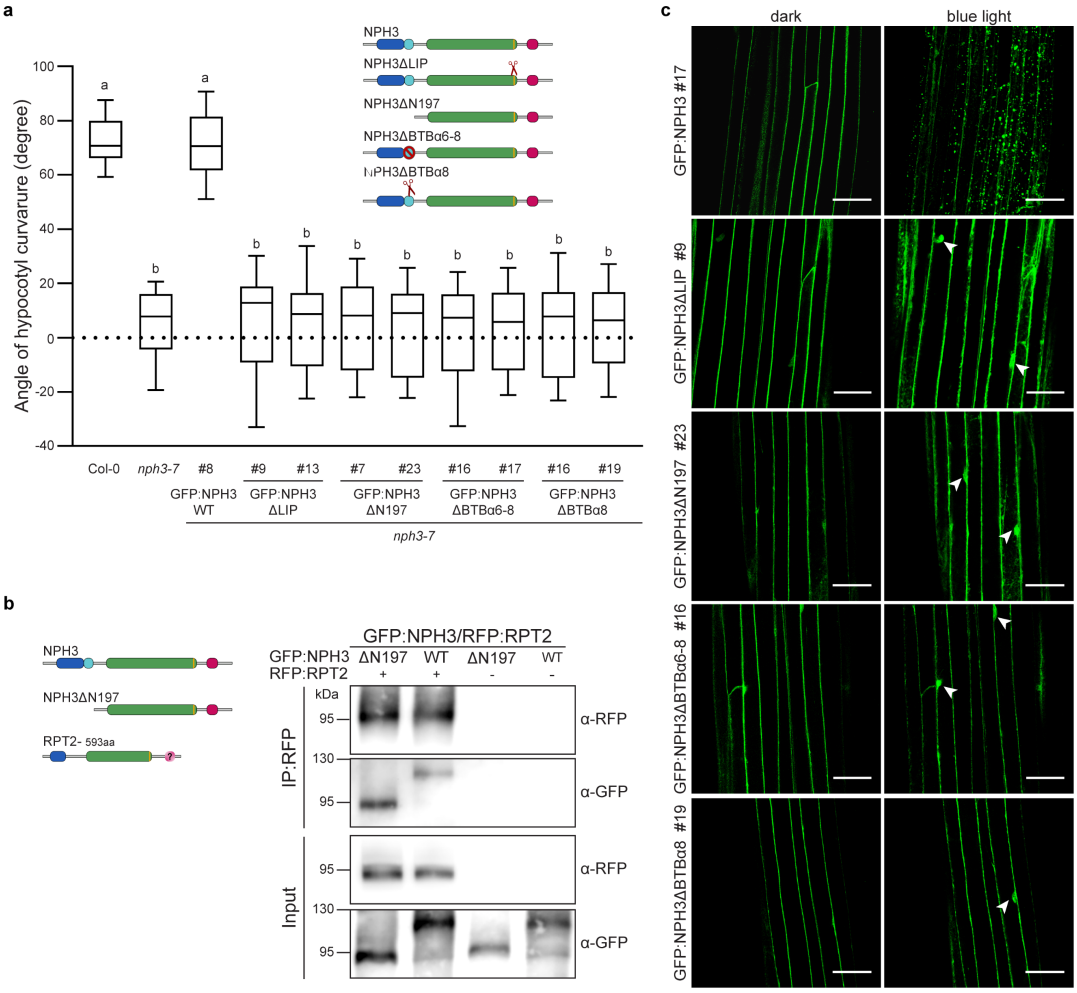

a Quantification of hypocotyl phototropism (mean ± SD) in etiolated *Arabidopsis nph3-7* seedlings ectopically expressing (35S promoter) GFP:NPH3 variants and exposed to unilateral blue light (BL) (1 µmol m^{-2} s^{-1}, 24 h) (n ≥ 30 seedlings per experiment, three replicates). One way ANOVA with Tukey's post-hoc test is shown, different letters mark statistically significant differences ($P < 0.05$). Centre line: median, bounds of box: minima and maxima (25th and 75th percentiles), whiskers: 1.5 × IQR (IQR: the interquartile range between the 25th and the 75th percentile). Exact *P*-values for all experiments are provided in the source data file. **b** *In vivo* interaction of GFP:NPH3 variants transiently co-expressed (35S promoter) with RFP:RPT2 in *N. benthamiana* leaves. The crude protein extract of dark-adapted tobacco plants was immunoprecipitated using RFP beads. Input and immunoprecipitated (IP:RFP) proteins were separated on 10 % SDS-PAGE gels, followed by immunoblotting with anti-GFP and anti-RFP antibodies, respectively. Experiments were performed at least two times with similar results. **c** Representative confocal microscopy images of hypocotyl cells from *Arabidopsis* seedlings shown in **a** and either maintained in darkness (dark) or treated with blue light (~ 11 min GFP laser). Scale bars, 50 µm. Experiments were performed at least two times with similar results. Arrowheads indicate nucleus.